
The Galactic Centre cloud G2 and scattering processes in the young stellar ring

Miriam Keppler



Munich 2013

The Galactic Centre cloud G2 and scattering processes in the young stellar ring

Bachelor thesis

at the

Ludwig–Maximilians–Universität München

by

Miriam Keppler

(Matr. nr.: 10392881)

born in Munich on 12/12/1990

supervised by

Prof. Dr. Andreas Burkert

and

Dr. Marc Schartmann

Munich, August 12, 2013

Evaluator: Prof. Dr. Andreas Burkert

Date for the oral examination: October 8, 2013

Contents

Introduction	1
1. The 'compact source' scenario	5
1.1. Constraints on a star embedded in G2	5
1.2. The young stellar ring	6
1.3. G2 as a photoevaporating protoplanetary disk	7
1.4. A T-Tauri star as compact source	9
2. First estimates from scattering theory	11
2.1. Two-body scattering	11
2.2. A simple analytical approach	13
2.2.1. Approximation for three-body problem	13
2.2.2. Cross section	15
2.2.3. Delivery rate	15
3. N-body simulations	18
3.1. Collisional and collisionless systems	18
3.2. REBOUND Code	19
3.3. Leapfrog Integrator	19
3.4. Initial Conditions	21
3.5. Timestep	24
3.6. Results	27
4. Discussion	29
4.1. Analytical calculations	29
4.2. Simulation	30
4.2.1. Delivery rates and probabilities	30
4.2.2. Single scattering encounters	30
4.2.3. Energy loss	31
4.2.4. Dynamical properties of perturber stars	32
4.2.5. Accuracy of timestep	32
Summary	34
Acknowledgements	37
A. Appendix	39

Bibliography	49
List of Figures	51
Statement of self-reliance	53

Introduction

A gas cloud is moving towards the super-massive black hole in the Galactic Centre of our Milky Way.

At a distance of 8.33 kpc, in the centre of our galaxy, resides a super-massive black hole (SMBH). It is identified with the central compact radio source, SgrA*. By monitoring stellar orbits in its direct environment, the gravitational potential which determines the motion of the nearby stars could be directly observed. With this approach a black hole mass of 4.31×10^6 times the mass of our sun was found (Gillessen et al., 2009).

In popular scientific terms, black holes often have a mystic status as 'cosmic vacuum cleaners' or 'energy monsters'. This association might come from the fact that at some distance to the black hole, the so-called 'Schwarzschild radius', even light is not able any more to escape the black hole's attracting force. For the case of SgrA* this corresponds to a distance of $\sim 1.3 \times 10^{10}$ m or 0.09 au. Further, when a black hole is accreting material, gravitational energy from infalling matter is released as thermal radiation, but also bremsstrahlung, synchrotron and cyclotron radiation can be detected from the environment of Active Galactic Nuclei.

Currently, the black hole in *our* galaxy has been remarkably faint. Its luminosity lies more than eight orders of magnitudes under its Eddington luminosity (Genzel et al., 2010). The Eddington luminosity corresponds to a maximum accretion rate which a black hole (or an accreting star) can reach under hydrostatic equilibrium - if the luminosity exceeds this limit, radiation pressure gains the upper hand and gravitational infall is diminished or even stopped. If accretion is non-spherical, e.g. in a disk, even super-Eddington accretion is possible. Hence, a low luminosity corresponds to a low accretion rate. But for the case of SgrA* things are potentially going to change: observations of the Galactic Centre indicate that the black hole is now going to be fed.

In 2011, while studying stellar orbits in the Galactic Center with the Very Large Telescope, Gillessen et al. (2012) discovered an object moving with a velocity of 1700 km/s on a nearly radial orbit towards SgrA*. Combining astrometric and

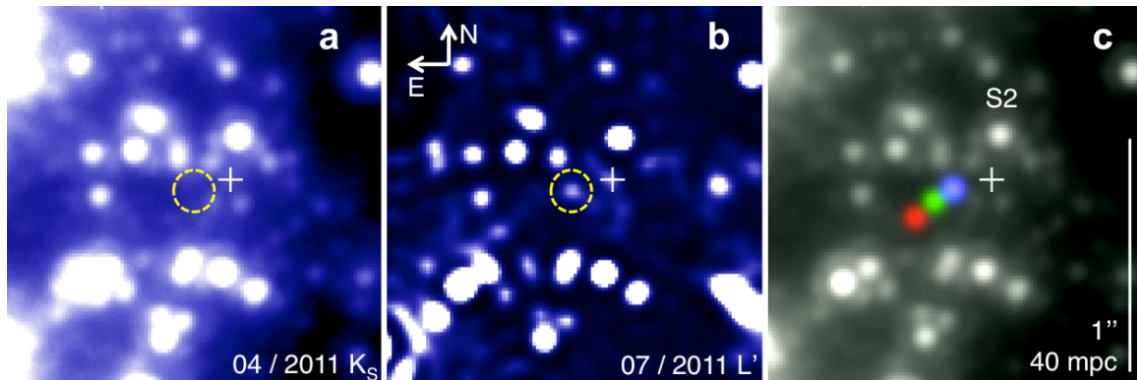


Fig. 0.1.: The cloud was observed in the L' -band (**b**), but not in the K_S -band (**a**) (dashed circles). Panel (**c**) shows the cloud's positions in 2004 (red), 2008 (green) and 2011 (blue). The cross marks the position of SgrA*. Adapted from Gillessen et al. (2012).

spectroscopic data, they found the object to be a dusty, ionized gas cloud having a mass of about three Earth masses and a radius of ~ 100 au. Dark, dusty clouds cover the view to the innermost of the Milky Way from Earth. Consequently, observations are mainly conducted in the infrared spectrum where dust is more transparent. The cloud (nick-named 'G2') was discovered in the L' -band ($3.76 \mu m$) and in the M-band ($4.7 \mu m$), but was not seen in the K_S -band ($2.16 \mu m$) (see Fig.0.1). According to this, a dust temperature of ~ 550 K could be estimated. Spectroscopically, G2 appears as a source of redshifted $Br\gamma$ and $Br\delta$ hydrogen, and $2058 \mu m$ He I emission which indicates that the cloud consists mainly of ionized gas. G2's discoverers were able to trace the cloud's orbit looking back into archival data of the last 10 years. They could see that the cloud is moving on a Keplerian orbit with a very high eccentricity of 0.97 and semi-major axis of about 5500 au implying an apocenter distance of 11000 au and a pericenter distance of only 190 au (corresponding to 2200 Schwarzschild radii) (Gillessen et al., 2013a). Also Phifer et al. (2013) could observe the cloud and derived an eccentricity of even 0.98 and a pericenter distance of 130 au. This is a remarkable value in view of the fact that only two stars have been detected at closer distances to the black hole so far (Gillessen et al., 2009). Observations show a growing velocity gradient along its travelling direction due to the tidal forces exerted by the gravitational potential of SgrA*. As a consequence, the cloud is already being stripped (see Fig.0.2).

Not only that G2 has started to stretch like a 'spaghetti' but also some fraction of the cloud seems to have already passed pericenter (Gillessen et al., 2013b). Nevertheless, it is assumed that the passage of closest approach to the black hole for the whole cloud will last for a period of about one year. This event will provide a unique

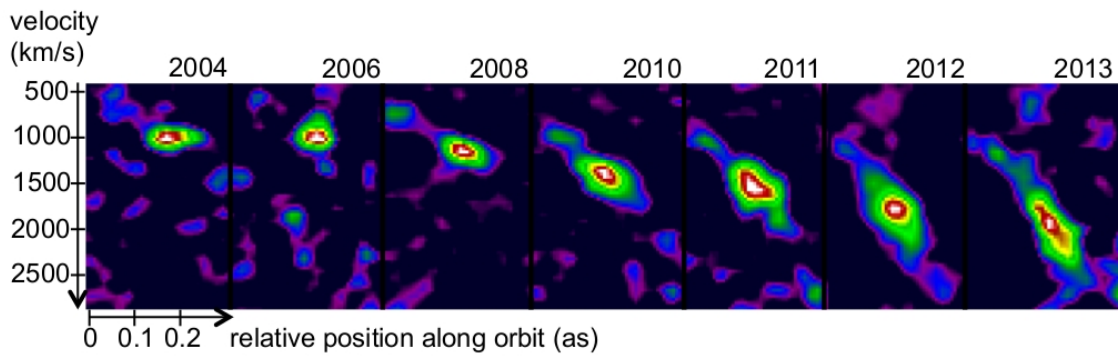


Fig. 0.2.: Position-velocity diagrams of G2 of the last couple years. The growing velocity gradient is clearly visible. Adapted from Gillessen et al. (2012).

opportunity to probe the physical conditions of the black hole's direct environment and will allow us to learn more about the properties of its accretion flow. To benefit from this astounding event, numerous observations are planned in a wide range of the electromagnetic spectrum ¹.

Given the extraordinary character of this observation it is reasonable to ask: what is actually the origin of the G2 cloud? And how could the cloud happen to reach such an unusual orbit? There are several propositions about the nature of G2: Gillessen et al. (2012) and Burkert et al. (2012) suggested that the cloud could have formed due to colliding winds produced by stars in the Galactic Centre environment. Schartmann et al. (2012) conducted hydrodynamical simulations to show that the evolution of a pure gas cloud having originally had a homogeneous or spherical shell-like structure on its way towards the black hole could match the observations. Meyer and Meyer-Hofmeister (2012) proposed that the cloud results from a recent nova outburst.

Two models, presented by Murray-Clay and Loeb (2012) and Scoville and Burkert (2013), suggest a compact source inside the cloud: a low-mass star which is too faint to be observable. Having originally been member of the disk of young, massive stars in the Galactic Centre, scattering events with its neighbours could have brought the star to its current orbit. But this opens a new question: how likely is such an orbital evolution?

In this bachelor thesis, I examine this question concerning the likelihood of scattering events in the young stellar ring leading to highly eccentric orbits. After having presented the two models about a compact source for G2 (chapter 1) I will exam-

¹see <https://wiki.mpe.mpg.de/gascloud/ProposalList>

ine scattering theory and make a first analytical approach to delivery rates in the young stellar ring (chapter 2). Finally, I run N-body simulations to elucidate scattering probabilities and will present procedure and results (chapter 3) followed by a discussion (chapter 4). I will finish the bachelor thesis with a summary.

1. The 'compact source' scenario

At first glance, the two models described by Murray-Clay and Loeb (2012) and Scoville and Burkert (2013) for a compact source of G2 are very similar: they both assume a low-mass stellar object inside the cloud which is too faint to be detected. This star originates from the disk of young stars around the Galactic Centre, and through gravitational interaction with massive perturbers it has been scattered on its highly eccentric orbit. Though, the physics of the cloud formation in the two scenarios is very different. In this chapter, I will briefly discuss the observed constraints on a potential star inside the cloud, then I will present the proposed origin of the star, namely the young stellar ring. Finally I will elaborate the details of the two different cloud formation processes.

1.1. Constraints on a star embedded in G2

No star is detected at the location where G2 is observed. Hence, it is to speculate which type of star could still be the source of G2, but without being detected. Observations of the Galactic Center yielded images of G2 at different wavebands. These can be used to infer constraints on the energy distribution of a possibly embedded star inside the cloud. As no emission is detected in the K_S -band, Gillessen et al. (2012) conclude a lower limit of 17.8 for the absolute magnitude in this waveband. Besides, they suggest the cloud to be optically thin to infrared radiation, so they can neglect that the stellar source could be hidden due to local extinction. These facts lead to two constraints on a star inside the cloud: it would be favourable if its temperature is high enough ($T > 10^{4.6}$ K) to shift its emission sufficiently in the UV spectrum. But at least its luminosity needs to be low enough ($L < 10^{3.7} L_{\odot}$) to lie below the detection limits. These constraints include for example sun-like low mass stars. Possible candidates are present in the young stellar ring.

1.2. The young stellar ring

The innermost of the Milky Way shows evidence of extreme properties that make the direct environment of the black hole a 'stellar collider' (Alexander, 2005): the close presence of the black hole causes extraordinarily strong tidal forces and accelerates stars to high velocities, and high stellar densities (in the central ~ 0.1 pc about a factor 10^9 higher than in the sun's neighbourhood) increase the rate of stellar collisions. The central parsec of our Galaxy can be divided into three stellar substructures (Alexander, 2005): in the innermost environment of the black hole, extending to a distance of ~ 0.04 pc, observations show evidence of a cluster of faint, blue stars, also called the 'S-cluster'. Their orbits seem to be randomly distributed in space. Jumping to some outer regions, outside ~ 0.4 pc, the stellar distribution goes slowly over into a large-scale mixed population of old and young stars.

Between these two populations, more precisely in a range of $6700 - 10^5$ au appears a configuration of young massive stars (Bartko et al., 2009). They are mainly identified as O, B and Wolf-Rayet stars and all have the property to be massive, hot and luminous. Especially the Wolf-Rayet (WR) stars are undergoing rapid mass loss by strong winds. Most of these stars reside in a clockwise-rotating disk which is part of a system containing two counter-rotating and strongly inclined rings. Already ~ 100 massive stars could be identified with observations. But also a few thousand low-mass stars down to masses of $0.3 M_{\odot}$ are assumed to be hosted by the young stellar ring. The orbits in the clockwise rotating disk are found to have an opening angle of $|h|/R \sim 10^\circ$, with h the scale height and R the local ring radius, and seem to be modestly eccentric (mean eccentricity ~ 0.35). The two disks probably formed from one or two massive gas clouds which were captured by the potential of the black hole some 10^6 years ago (Bonnell and Rice (2008), Alig et al. (2011), Alig et al. (2013)). By examining the fractions of its star populations, the age of the disk system could be estimated to ~ 6 My.

Now, what is the link between the G2 cloud and this stellar system? The observations gave a remarkable result: the plane of the cloud's orbit coincides with that of the clockwise rotating disk, and further, its apocenter distance (~ 11000 au) lies well within the inner part of the young stellar ring. This led Murray-Clay and Loeb (2012) and Scoville and Burkert (2013) to their presumption, that the low-mass star originally belonged to the ring, and was scattered to its plunging orbit.

1.3. G2 as a photoevaporating protoplanetary disk

Most of the stars in a cluster are initially equipped with proto-planetary disks (Haisch et al., 2001). A good fraction of these disks gets lost within a period of 3 My whereas some stars may hold them for up to 6 or even 10 My. The extend of circumstellar disks can reach a few hundred au (Natta, 2004).

In the scenario of Murray-Clay and Loeb (2012), the star is surrounded by such a protoplanetary disk. It consists of cold dust and gas of temperatures ~ 300 K, so that the disk itself can't be observed. Assuming an initially circular orbit for G2 with approximately the radius of its current apocenter distance (11000 au), they argue that a solar mass star can be able to host a proto-planetary disk on its original orbit. Their argumentation goes as follows: consider a test particle surrounding the low-mass star. Due to the gravitational force of the black hole, there is one outermost orbit radius for which the particle is still bound to its host. The corresponding radius is called *Roche radius*. It can be calculated as follows (Binney and Tremaine, 2008):

$$r_{\text{roche}} = \left(\frac{m_*}{3M_{BH}} \right)^{\frac{1}{3}} d_0 \approx 50 \text{ au} \left(\frac{m_*}{M_\odot} \cdot \frac{4.31 \times 10^6 M_\odot}{M_{BH}} \right)^{\frac{1}{3}} \quad (1.1)$$

with $d_0 \approx 11000$ au being the distance between the star and black hole on its initial orbit, m_* and M_{BH} the masses of the low-mass star and the black hole respectively. Murray-Clay and Loeb (2012) argue, that a star could then host a stable disk with radius $\sim r_{\text{roche}}/3$. This would mean, that a solar-mass star could hold a stable disk with radius $r_{\text{disc}} \sim 17$ au, and a star of mass $0.3M_\odot$ could be surrounded by a disk with radius $r_{\text{disc}} \sim 9$ au.

During its evolution in the young stellar ring, the star experiences scattering events from neighbour stars at different distances that bring it to its low angular momentum orbit. The configuration of the system can be seen in Fig.1.1 (left). Since later, the cloud will be formed from disk material, it is important that these encounters occur on such distances, that the disk is not stripped or even destroyed by tidal forces. Therefore, Murray-Clay and Loeb (2012) (Supplementary Discussion) calculate a minimal impact parameter of ~ 10 au which ensures the disk not to be disrupted during the scattering process.

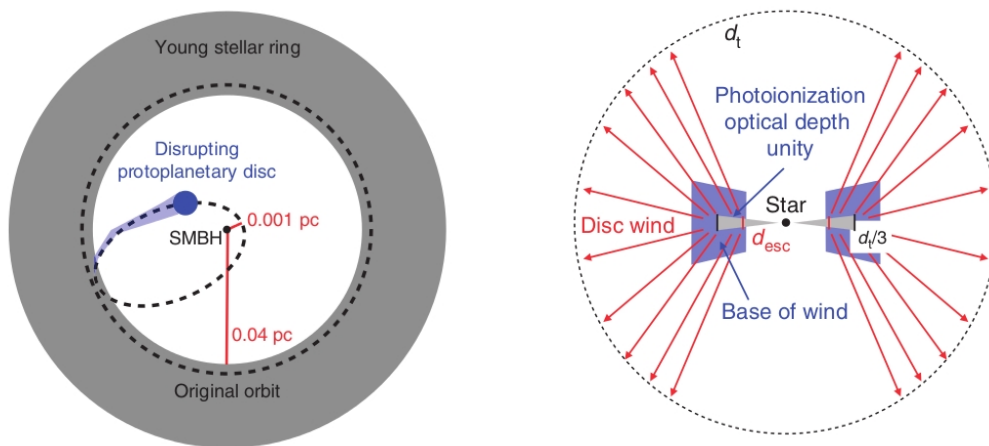


Fig. 1.1.: In the model of Murray-Clay and Loeb (2012), G2 originates from the inner part of the young stellar ring and is scattered to its plunging orbit (left). Photoevaporation and growing tidal forces then disrupt the disk and lead to the formation of a dusty gas cloud, G2 (right). Adapted from Murray-Clay and Loeb (2012).

Now, during its plunge towards the black hole, there are two mechanisms that lead to mass loss from the disk and finally to the formation of the cloud:

The star's Roche radius shrinks as it approaches the black hole. In the end, at pericenter, it will be only $\sim 1 \text{ au} (m_*/M_\odot)^{\frac{1}{3}}$. Whatever is outside the Roche radius is going to get stripped away and forms a cloud of debris around the star. As a consequence, both, the disk and also the cloud, are tidally stretched and more and more material is disrupted. So, an increasing amount of particles contributes to the formation of the cloud and to its emission. From this point, Murray-Clay and Loeb (2012) expect a significant increase of the total $\text{Br}\gamma$ luminosity during the cloud's plunge towards the Galactic Centre.

Further, the Galactic Centre shows evidence of ionizing and far ultraviolet (FUV) photons from the nearby hot and massive stars. This high-energy radiation heats the surface of the disk. If the thermal velocity $v_{\text{th}} \sim \sqrt{\frac{k_B T}{m_{\text{particle}}}}$ exceeds the local escape velocity $v_{\text{esc}} \sim \sqrt{\frac{Gm_*}{d_{\text{esc}}}}$ at a distance d_{esc} , then particles are lifted from the disk and also form a dusty and gaseous cloud around the star (see Fig.1.1, right). These calculations lead the authors to assume that material is lifted from an inner extend of about 10 to 100 au.

During gravitational encounters or pericenter passages the cloud and even parts of the disk may be disrupted. But as long as some material is left on the disk, the cloud can be regenerated. The current pericenter passage will be critical, though: disk and cloud material out of $\sim 1 \text{ au}$ could be disrupted. In any case, the star itself

will survive pericenter passage, tidal forces will significantly truncate the disk and hence the cloud generating wind should at least be reduced for some time.

This model can account for the observed size and emission properties of the G2 cloud. But, current observations did not show the expected increase of emission so far, on the contrary, following Gillessen et al. (2012), it has stayed constant during the last years.

1.4. A T-Tauri star as compact source

Also in the model presented by Scoville and Burkert (2013), the G2 cloud is formed around a low-mass, young-aged, and still disk-surrounded star. It originally belonged to the young stellar ring and has been scattered inwards to the Galactic Nucleus. So far, identical to the model above. The difference comes with the formation of the cloud: the star is currently in the so-called T-Tauri phase which is one of the last stages for sun-like stars before main sequence life starts. At this time, the star undergoes strong winds from the inner edge of its disk with wind velocities of order 100 km/s. After being scattered inwards towards the Galactic Centre the star dives into the hot, X-Ray emitting gas which is present in the innermost of the Galaxy. In general, every body which is moving through a fluid or a gaseous medium undergoes a drag force due to ram pressure as the medium on its front is compressed. The ram pressure is of order (Binney and Tremaine, 2008)

$$P = \rho v^2 \quad (1.2)$$

with ρ the density of the ambient medium and v the velocity of the body. Consequently, as the star approaches the Galactic Centre, the hot gas exerts ram pressure on the star: $P_{\text{gas}} = \rho_{\text{gas}} v_*^2$. This is countered by the pressure of the outflowing T-Tauri-wind: $P_{\text{wind}} = \rho_{\text{wind}}(r) v_{\text{wind}}^2 = \left(\dot{M} / (4\pi r^2 v_{\text{wind}}) \right) v_{\text{wind}}^2$. Hence, the point in front of the star where these two pressures are in equilibrium $P_{\text{gas}} = P_{\text{wind}}$ is at distance r_{equi} from the star

$$r_{\text{equi}}^2 = \frac{\dot{M} v_{\text{wind}}}{4\pi \rho_{\text{gas}} v_*^2}. \quad (1.3)$$

Choosing typical values for T-Tauri stars, $\dot{M} = 4 \times 10^{-8} M_{\odot}$, $v_{\text{wind}} = 100$ km/s, and for the hot ambient gas, $\rho_{\text{gas}} = 10^{-21}$ g/cm³ and assuming a stellar velocity of 2000 km/s, Scoville and Burkert (2013) compute $r_{\text{equi}} \sim 14$ au. Hence, at this location,

the wind is stopped and a strong shock front occurs, consisting of two layers: the stellar wind meets the compressed gas at r_{equi} producing a *cold* shock front; this in turn meets the hot ambient gas farther outside causing a *hot* bow shock. The configuration can be seen in Fig.1.2.

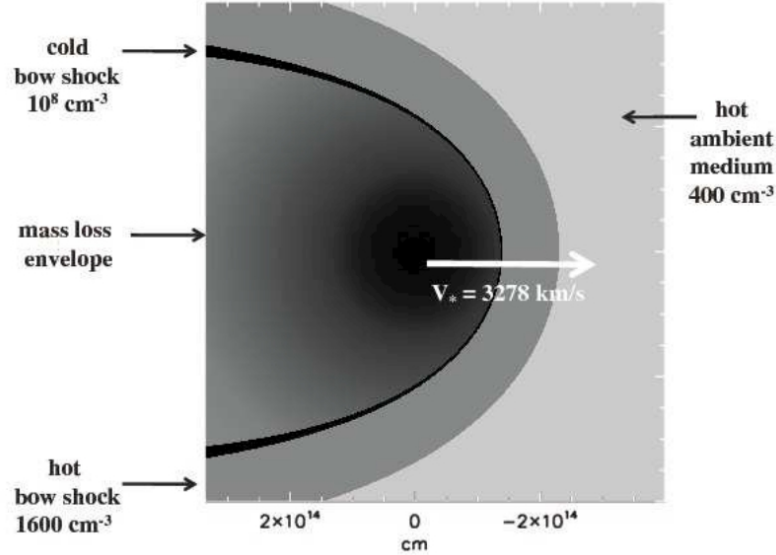


Fig. 1.2.: As the T-Tauri star moves through the hot ambient gas, ram pressure due to the interaction of the T-Tauri wind and the gas leads to the formation of a shock front. Adapted from Scoville and Burkert (2013).

In this scenario, the observed cloud emission lines come from the shock front region: wind material passing the bow shock lead to collisional ionization of the medium. On this way, the observed constancy of the line flux can be explained: since mass-loss rate and velocity of the T-Tauri wind are insensitive on the distance to SgrA*, also the ionization rate and hence emission line flux are a pure function of the stellar parameters which causes the observed constancy of luminosity. Since the wind launching region ($\sim 0.2 \text{ au}$) on the inner range of the disk is small compared to the Roche radius at pericenter distance (of order 1 au , see section 1.3) the wind and hence the cloud should not be destroyed during the closest approach period. So G2 should survive and stay observable after pericenter passage.

2. First estimates from scattering theory

For both models, the same question occurs: how likely is the transport of a low-mass star originated from the young stellar ring to such a highly eccentric orbit? The aim of this chapter is to make a rough estimation on delivery rates to G2-like orbits.

2.1. Two-body scattering

The gravitational interaction of two bodies, m_1 and m_2 , moving initially with relative velocity v_{rel} can be simplified by splitting the system into the motion of the center of mass and the motion of the bodies relative to it (see Landau and Lifshitz (1966)). Hence, the system is described by the movement of a *reduced* particle with mass $\mu = \frac{m_1 m_2}{m_1 + m_2}$ in a central potential generated by the mass $M = m_1 + m_2$ which is fixed in the origin. For this so-called *Keplerian problem* exists an exact solution. The orbit of the reduced particle is described by

$$\rho = \frac{L^2}{\mu\alpha(1 + \epsilon \cos(\varphi))} \quad (2.1)$$

with $\alpha \equiv Gm_1 m_2$, L the angular momentum of the reduced particle, $\epsilon = \sqrt{1 + \frac{2EL^2}{\mu\alpha^2}}$ the *eccentricity*, φ the current angle with respect to the semi-major axis, and ρ the time-dependend radial distance to the origin (see Fig.2.1). For total energy $E < 0$ is $\epsilon < 1$, and the particle does not have enough energy to escape. It is bound on a closed, elliptical orbit. In the case where $E > 0$, the particle follows a hyperbolic orbit and is able to escape to infinity.

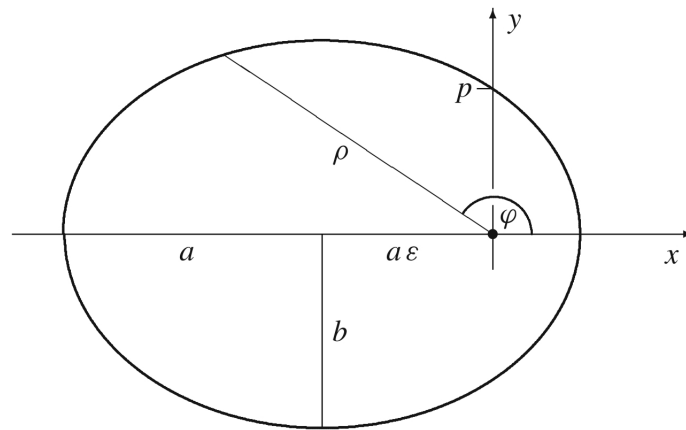


Fig. 2.1.: Bound, elliptical orbit in the Keplerian problem. Adapted from Fliessbach (2009).

During a two-body scattering process, the total energy of the system is conserved, as well as angular momentum. Additionally, in case that no external potential is present and if the scattering is elastic, energy conservation is also valid for each particle itself (m_1 and m_2 or μ and M respectively). As a consequence the absolute value of the scattered particle's velocity before the gravitational encounter equals that after the scattering ($|\vec{v}_0| = |\vec{v}'|$). It is useful to introduce the *impact parameter* b which is the perpendicular distance of the particle's orbit at $\rho \rightarrow \infty$ with respect to the center.

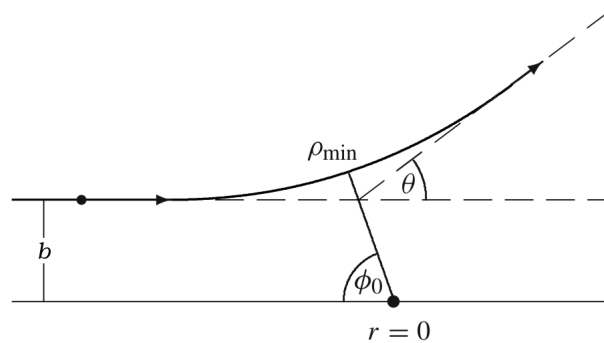


Fig. 2.2.: Hyperbolic orbit during two-body scattering (for a repulsive potential). Adapted from Fliessbach (2009).

As long as the reduced particle is at infinite distance (that means before any significant gravitational interaction occurs), its angular momentum can be written as $L = \mu b v_{\text{rel}}$. From equation 2.1, its orbital angle computes as $\Phi_0 \equiv \Phi(\rho \rightarrow \infty) = \arccos\left(\frac{1}{\epsilon}\right)$. By introducing the scattering angle $\theta = \pi - 2\Phi_0$ (see Fig.2.2), and

remembering that ϵ depends through L on b and v_{rel} , one can establish a connection between the impact parameter and the scattering angle:

$$b(\theta) = \frac{G(m_1 + m_2)}{v_{\text{rel}}^2} \cot\left(\frac{\theta}{2}\right) \quad (2.2)$$

2.2. A simple analytical approach

Now, how do scattering processes look like in the young stellar ring? To keep things as simple as possible, I will consider only scattering encounters that bring the cloud to its highly eccentric orbit via one single scattering event. Having just considered the Keplerian problem, the situation for scattering in the young stellar ring turns out to be more complicated: a dominant external potential, namely that of the black hole, is present and changes the configuration from a two-body configuration to a three-body problem. In general, such a problem can't be solved analytically. To get an impression though, I will make the following approximations.

2.2.1. Approximation for three-body problem

Let's assume a low-mass star with $m_* = 1M_{\odot}$ moving initially on a circular orbit with radius $r_* \sim 11000$ au and a velocity $v_* = \sqrt{\frac{G(M_{\text{BH}} + m_*)}{r_*}} \approx 590$ km/s. A single scattering event which brings the cloud to high eccentricity needs to be quite strong and hence is more effective the higher the perturber's mass. Observations on the young stellar ring show evidence of stars up to $60 M_{\odot}$ (see section 2.2.2, below), so let's assume this value as the perturber mass. In my model, this massive star is orbiting with a typical eccentricity of 0.35. As it spends a good fraction of its time on apocenter, I assume it to be most likely that scattering takes place during this period, and adopt an apocenter distance of 11000 au for the perturber star (see Fig.2.3). At this location, it moves with velocity $v_{\text{pert}} = \sqrt{\frac{G(M_{\text{BH}} + m_{\text{pert}})(1-\epsilon)}{r_{\text{apo}}}} \approx 480$ km/s. Hence, the two stars have a relative velocity of 110 km/s at the perturber's apocenter.

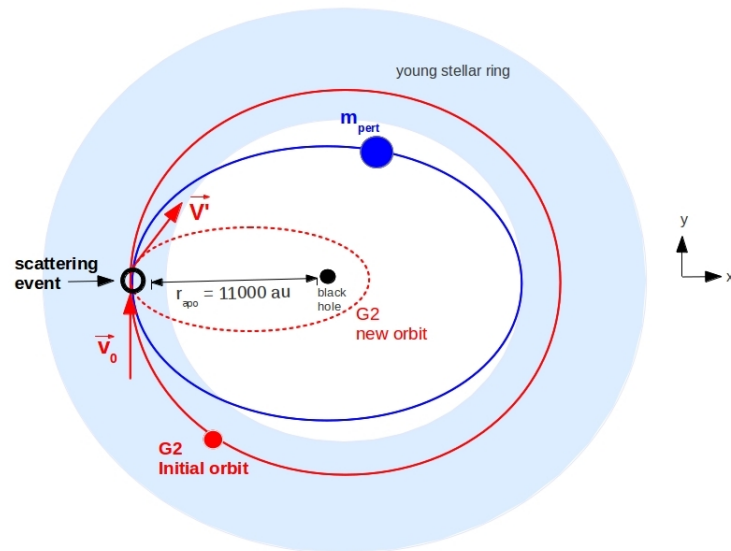


Fig. 2.3.: Sketch of the scattering configuration in my approximated calculations. Scattering takes place for an infinitely short time at the perturber's apocenter.

The question now is: which scattering angle and hence which impact parameter would lead to a change in eccentricity of $\epsilon_* \sim 0.9$ for the low-mass star? To estimate this, I consider the following scattering process: initially, the two stars are orbiting the black hole without any respective gravitational interaction. As the perturber star reaches apocenter, the potential of the black hole is turned off, and the two stars are now gravitationally interacting. Hence, the scattering process itself takes place without any external potential. Further, I assume that the length scale of the respective gravitational interaction is negligibly small compared to the whole system, so that the scattering can be approximated as a point-like event. Right after the perturber has left apocenter, the scattering is fulfilled and the gravitational field of the black hole can be turned on again. Now, the stars are moving again on constant orbits, but without any respective interaction. As in my system during scattering itself no black hole field is present, I can treat it as a two-body problem and hence can assume energy conservation for each of the two stars.

The new, post-scattering eccentricity ϵ'_* of the low-mass star depends on its energy E'_* and angular momentum L'_* (see section 2.1). Let's evaluate these values. Before scattering, the energy of the low mass star is

$$E_*^0 = \frac{1}{2}\mu_{BH}v_*^2 - \frac{GM_{BH}m_*}{r_*} = E'_*, \quad (2.3)$$

where identification $E_*^0 = E_*'$ is due to energy conservation. $\mu_{BH} = \frac{M_{BH}m_*}{M_{BH}+m_*}$ denotes the reduced mass of the system black hole – low mass star. Further, as explained in section 2.1, during two-body scattering, the absolute value of velocity of each star remains constant. Only its direction changes, from $\vec{v}_{*,0} = (0, v_*)$ to $\vec{v}'_* = (v_*\sin\theta, v_*\cos\theta)$. Hence, the angular momentum right after scattering reads:

$$|\vec{L}'_*| = \mu_{BH} |\vec{r}_{\text{apo}} \times \vec{v}'_*| = |\mu_{BH} r_{\text{apo}} v_* \cos\theta| \quad (2.4)$$

Combining (2.3) and (2.4), one gets the new eccentricity with respect to the black hole:

$$\epsilon'_* = \sqrt{1 + \frac{2E'_* L_*'^2}{\mu_{BH} \alpha^2}} = \dots = \sqrt{1 - \cos(\theta)^2} \quad (2.5)$$

To reach an eccentricity of 0.9, a scattering angle of $\sim 65^\circ$ is required.

2.2.2. Cross section

From particle scattering theory, I can now compute the cross section:

$$d\sigma = 2\pi b db = 2\pi b(\theta) \left| \frac{db(\theta)}{d\theta} \right| d\theta = 2\pi \left(\frac{G(m_{\text{pert}} + m_*)}{v_{\text{rel}}^2} \right)^2 \frac{\cos(\theta/2)}{\sin(\theta/2)^3} d\theta. \quad (2.6)$$

For a scattering event transporting the low-mass star to $\epsilon'_* > 0.9$ it results

$$\sigma = 2\pi \int_{65^\circ}^{90^\circ} \left(\frac{G(m_{\text{pert}} + m_*)}{v_{\text{rel}}^2} \right)^2 \left(\frac{\cos(\theta/2)}{\sin(\theta/2)^3} \right) d\theta \quad (2.7)$$

$$\approx 4.1 \times 10^{24} \text{ m}^2 \left(\frac{(m_{\text{pert}} + m_*)}{61M_\odot} \right)^2 \left(\frac{v_{\text{rel}}}{110 \text{ km/s}} \right)^{-4}. \quad (2.8)$$

Obviously, the cross section is proportional to m_{pert}^2 which means that scattering processes are dominated by high-mass perturbers.

2.2.3. Delivery rate

From this point, a scattering rate f per low-mass star can be calculated via

$$f = n\sigma v_{\text{rel}}. \quad (2.9)$$

The only value which needs to be yet computed is the number density n of perturber stars in the inner region of the young stellar ring.

The best fit for the radial surface density (number dN of stars on surface $2\pi r dr$) of the clockwise stars results in a power law $\Sigma(r) \propto r^{-1.4}$ (Bartko et al., 2009). The mass function describing the number of stars N with mass m , follows the law $\frac{dN}{dm} \propto m^{-0.45}$ for massive stars from $7 M_{\odot}$ to an upper observed limit of $60 M_{\odot}$; below this mass range ($0.3 - 7 M_{\odot}$) it can be described by the Salpeter initial mass function $\frac{dN}{dm} \propto m^{-2.35}$ (Murray-Clay and Loeb, 2012). In total, a mass of $M_{\text{total}} \sim 10^4 M_{\odot}$ is associated with the young stellar ring. As $N \propto \int \frac{dN}{dm} dm \propto m^{0.55}$ for massive stars, and $M_{\text{total}} \propto \int N m dm \propto \int m^{1.55} dm$ it follows, that the largest fraction of mass is concentrated in the massive stars (see Fig.2.4).

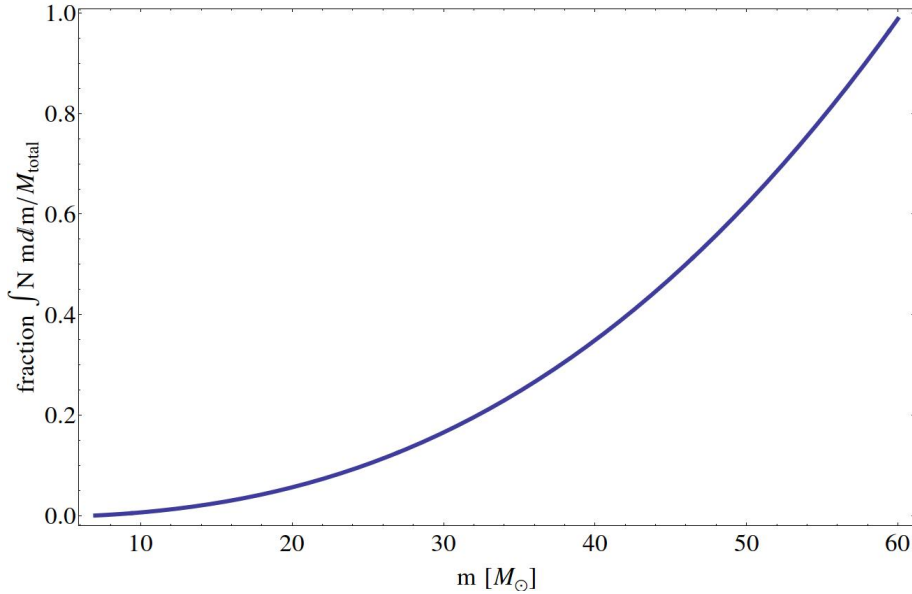


Fig. 2.4.: Plot of mass fraction contained in stars up to mass m with respect to the total mass of the young stellar ring. It can be seen that nearly 50% of mass is included in stars between 50 and $60 M_{\odot}$.

For this reason, about $10^4 M_{\odot} / 60 M_{\odot} \sim 170$ massive stars of $60 M_{\odot}$ could reside in the ring (compare Murray-Clay and Loeb (2012)). Not the whole disk but only the neighbourhood of the cloud's apocenter where the scattering takes place, let's say a range between 6700 and 20000 au, is of interest here. So, what fraction of perturber stars would we find in this region? That is calculated from the surface density by $\frac{N_{\text{inner range}}}{N_{\text{whole disk}}} = \frac{\int_{6700 \text{ au}}^{20000 \text{ au}} r^{-1.4} r dr}{\int_{6700 \text{ au}}^{10^5 \text{ au}} r^{-1.4} r dr} \approx 0.25$, hence $N_{\text{pert}} = 170/4 \sim 40$ high-mass stars could be found near the cloud's apocenter.

What about the amount of low mass stars? As $N = A \times m^{0.55}$ for a range of 7 - 60 M_{\odot} and $N = B \times m^{-1.35}$ for 0.3 - 7 M_{\odot} with A and B being constants, $N(60 M_{\odot}) = 40 = A \times 60^{0.55}$ perturbers reside the inner part of the ring. This results in $A \sim 4.2$. Knowing A now, $A \times 7^{0.55} \approx 12 \approx B \times 7^{-1.35}$ stars of 7 M_{\odot} can be found. It follows $B \sim 166$. So, $B \times 1^{-1.35} \approx 170$ stars of 1 M_{\odot} and $B \times 0.3M_{\odot}^{-1.35} \approx 900$ stars of 0.3 M_{\odot} could be hosted by the inner part stellar ring.

Back to the number density of perturber stars. The volume of the inner range of the ring can be estimated as a cylindrical ring form: $V = \pi(R_2^2 \times 2h(R_2) - R_1^2 \times 2h(R_1))$ with $R_2 = 20000$ au and $R_1 = 6700$ au. The scale height at radius R is $\sim 10^{\circ} \times R$ (see section 1.2), hence $h(R_1) \sim 1200$ AU and $h(R_2) \sim 3500$. The number density of perturber stars is

$$n = \frac{N_{pert}}{V} \sim 4.7 \times 10^{-12} \text{au}^{-3} \approx 1.4 \times 10^{-45} \text{m}^{-3} \quad (2.10)$$

In total, these calculations give a scattering rate for a single star of $\sim 2 \times 10^{-8} \text{yr}^{-1}$ for both types, $1M_{\odot}$ and $0.3M_{\odot}$ stars. According to their populations of 170 and 900 stars respectively, this corresponds to a delivery rate of $f \times 170 \approx 3 \times 10^{-6} \text{yr}^{-1}$ for $m = 1M_{\odot}$ and one of $f \times 900 \approx 2 \times 10^{-5} \text{yr}^{-1}$ for $m = 0.3M_{\odot}$. In summary, about 20 $1M_{\odot}$ stars and 108 $0.3M_{\odot}$ stars could be delivered onto highly eccentric orbits up to the current age of the stellar ring. This makes roughly 10 % of each population.

3. N-body simulations

To get more reliable answers about scattering processes in the young stellar ring, it is reasonable to carry out N-body simulations. The configurations of the simulations is similar to those conducted by Murray-Clay and Loeb (2012). They include the super massive black hole (of mass $4.3 \times 10^6 M_\odot$), the inner part of the young stellar ring represented by 40 massive perturbers of $60 M_\odot$ each, and 900 test particles which correspond to the low-mass stars (see section 2.2.3 for a detailed derivation of population numbers). The initial conditions for each star are randomly set according to the properties of the young stellar ring. To get a statistical conclusion, 10 simulations with different random realisations of the initial conditions are launched. But before being able to start, an appropriate code has to be found.

3.1. Collisional and collisionless systems

Gravitational systems can be divided in two classes: collisional and collisionless systems. The deciding parameter therefore is the *relaxation time* t_{relax} . This is the time after which sufficient gravitational encounters have taken place to have changed a star's initial orbit on a significant way. So, if the stellar system is relaxed (that means $t > t_{\text{relax}}$), informations about the orbit's initial conditions have been washed out.

For collisional systems, t_{relax} is short compared to their age so that gravitational encounters have been playing an important role for the evolution of the system. So, in this case it is recommendable to use a *collisional* N-body code which computes the forces exerted by all included mass points by direct summation. In contrast, if timescales $\lesssim t_{\text{relax}}$ are considered, the system can be treated as a collisionless system. Gravity is by far the weakest, but most long-range of the fundamental forces. Hence, in the case where close gravitational encounters do not play an important role, the potential can be approximated by a smooth mean potential. This saves significant computation cost in contrast to direct summation methods

(see Binney and Tremaine (2008)).

The relaxation time for the young stellar ring is estimated to be of order 10^9 yr Alexander (2005). Considering its age of ~ 6 Myr we are formally concerned with a not relaxed, collisionless system. But in the simulations, rare scattering events which hardly influence the dynamics of the ring system as a whole, are of special interest as they are the mechanisms that could bring stars onto highly eccentric orbits. Hence, it is the most appropriate to use a *collisional* N-body code. For this bachelor thesis, the REBOUND code has been chosen.

3.2. REBOUND Code

REBOUND is an open-source¹ N-body code for collisional systems entirely written in C (Rein and Liu, 2012). It was originally designed to simulate processes in systems like planetary rings (Rein and Latter, 2013), (Latter et al., 2012) or planetary formation (Paardekooper et al., 2013) but due to its high modularity it can be used for a variety of problems in astrophysics. Several different modules concerning gravity, collisions and boundary conditions are available. One can determine a certain time interval for which positions, velocities and orbital parameters of each particle are put out in an ASCII-file. To accelerate computation, it is possible to run the processes fully parallelized with MPI as well as with OpenMP. Furthermore, a real-time 3D-visualization using OpenGL can be enabled. With REBOUND, three different integrators are available: Leapfrog, the symplectic epicycle integrator (SEI), and a Wisdom-Holman mapping. After having tested several of them, I decided to use the Leapfrog integrator.

3.3. Leapfrog Integrator

The aim of my simulations is to compute the motion of the stars in the young stellar ring (represented as point masses) in the potential of the super-massive black hole and under their mutual gravitational interaction. This is a classical N-body problem. Such a system is governed by the Hamiltonian

$$H = T(\vec{p}) + \Phi(\vec{r}) = \sum_{i=1}^N \frac{\vec{p}_i^2}{2m_i} - G \sum_{i=1}^N \sum_{j>i}^N \frac{m_i m_j}{|\vec{r}_i - \vec{r}_j|}. \quad (3.1)$$

¹<https://github.com/hannorein/rebound>

with T and Φ being the total kinetic and potential energy; \vec{p}_i the momentum and \vec{r}_i the position of particle i . By solving the equations of motion

$$\dot{\vec{r}}_i = \frac{\partial H}{\partial \vec{p}_i}, \quad (3.2)$$

$$m_i \ddot{\vec{r}}_i = \dot{\vec{p}}_i = -\frac{\partial H}{\partial \vec{r}_i} \quad (3.3)$$

one can calculate the evolution of position and momentum with time. As there is no analytical solution for the N-body problem including more than two particles, the task for an orbit integrator is to solve iteratively the equations of motion for each timestep $t_n = t_0 + n\Delta t$. There are several methods to do so by direct summation of the occurring forces (Dehnen and Read, 2011). The simplest one is the so-called *Euler method* which corresponds to a Taylor expansion of position and velocity in time to first order in Δt . An often used method to increase accuracy is the so-called *Leapfrog* integrator. It is applied in a wide range of fields like stellar dynamics, plasma physics, and molecular dynamics (Hut et al., 1995). Leapfrog is a symplectic integrator which means that it exactly solves an approximated Hamiltonian $\tilde{H} = H + H_{err}$. A property of symplectic integrators is to preserve phase-space volume and Poincaré invariants which implies total energy conservation (Binney and Tremaine, 2008).

The leapfrog integration scheme goes as follows:

$$\vec{r}\left(t + \frac{\Delta t}{2}\right) = \vec{r}(t) + \frac{\Delta t}{2}\vec{p}(t) \quad (3.4)$$

$$\vec{p}(t + \Delta t) = \vec{p}(t) - \Delta t \vec{\nabla}\Phi\left(\vec{r}\left(t + \frac{\Delta t}{2}\right)\right) \quad (3.5)$$

$$\vec{r}(t + \Delta t) = \vec{r}\left(t + \frac{\Delta t}{2}\right) + \frac{\Delta t}{2}\vec{p}(t) \quad (3.6)$$

This integration method is also called 'drift-kick-drift' algorithm because in the first part (3.4) only position is changed ('drift'), followed by a change in momentum ('kick') (3.5), and the whole timestep is finished by again fulfilling a drift operation (3.6). In the limit $\Delta t \rightarrow 0$ this scheme solves the exact Hamiltonian H .

An appealing property of Leapfrog is its second-order accuracy in Δt , in contrast to the first-order Euler method. Besides, Leapfrog is time reversible which suppresses numerical dissipation.

3.4. Initial Conditions

Now, initial conditions have to be set. A Keplerian orbit is uniquely identified by 6 elements: eccentricity ϵ , semimajor axis a , inclination i , longitude of ascending node Ω , argument of periapsis ω , and true anomaly ν . ϵ and a define the shape of the ellipse, while i (angle of orbital plane with respect to x-y plane) and Ω (angle in x-y plane from positive x-axis to ascending node) describe the orientation of the orbital plane in space. Finally, the parameter ω (angle from direction of ascending node to pericenter distance) defines the orientation of the ellipse in its plane and ν (angle of orbiting star with respect to pericenter distance) implies the current position of the object on its orbit. The parameters are illustrated in Fig.3.1.

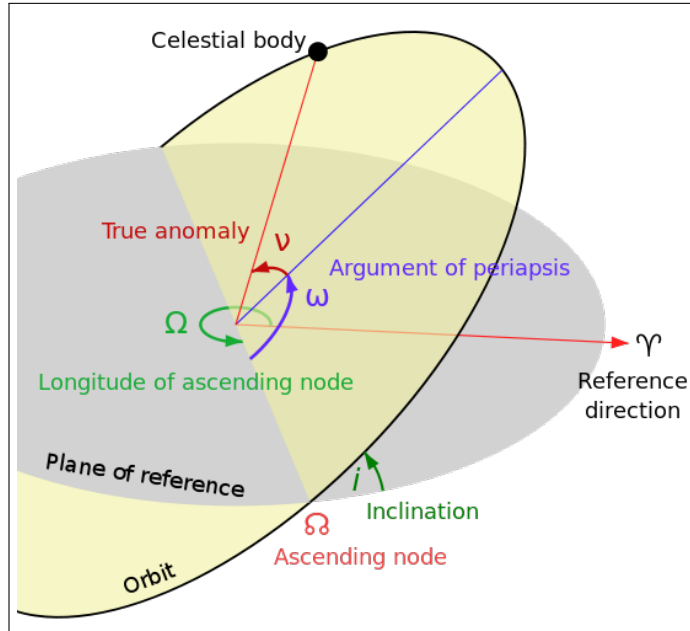


Fig. 3.1.: Orbital elements of Keplerian orbit. Adapted from Wikipedia (2010).

To set the initial conditions in the code, the orbital parameters have to be expressed as cartesian coordinates. To do this, the following considerations are important: given ϵ and a , the orbit can be drawn in xy-plane. Identifying semi-major axis with the x-axis and pericenter showing to positive x-axis this can be done from the orbital equation (compare equation (2.1))

$$\rho(t) = \frac{p}{1 + \epsilon \cos(\nu)}, \quad (3.7)$$

with $p = a(\epsilon^2 - 1) = \frac{L^2}{\mu\alpha}$ called *parameter*. Each point on this orbit can be reached by

$$\vec{q} = \begin{pmatrix} \rho \cos(\nu) \\ \rho \sin(\nu) \end{pmatrix} = \begin{pmatrix} \frac{p \cos(\nu)}{1 + \epsilon \cos(\nu)} \\ \frac{p \sin(\nu)}{1 + \epsilon \cos(\nu)} \end{pmatrix}. \quad (3.8)$$

Taking the derivative with respect to time, one gets

$$\dot{\vec{q}} = \frac{p\dot{\nu}}{(1 + \epsilon \cos(\nu))^2} \begin{pmatrix} -\sin(\nu) \\ \cos(\nu) + \epsilon \end{pmatrix}. \quad (3.9)$$

Since in general, orbits are not embedded in the x-y plane the ellipse has to be placed in space. Therefore three rotation transformations are carried out: rotate the orbit by ω around the z-axis, then by i around x-axis, and finally by Ω again around the z-axis. These calculations result in

$$\vec{r} = \begin{pmatrix} x \\ y \\ z \end{pmatrix} = R_z(\Omega)R_x(i)R_z(\omega) \cdot \vec{q} = \quad (3.10)$$

$$\begin{pmatrix} (\cos(\Omega)\cos(\omega) - \cos(i)\sin(\Omega)\sin(\omega))q_x - (\sin(\Omega)\cos(\omega)\cos(i) + \cos(\Omega)\sin(\omega))q_y \\ (\sin(\Omega)\cos(\omega) + \cos(\Omega)\sin(\omega))q_x + (\cos(\Omega)\cos(\omega)\cos(i) - \sin(\Omega)\sin(\omega))q_y \\ \sin(\omega)\sin(i)q_x + \cos(\omega)\sin(i)q_y \end{pmatrix}. \quad (3.11)$$

To calculate $\dot{\vec{r}}$ now, \vec{q} , q_x and q_y simply have to be replaced by $\dot{\vec{q}}$, \dot{q}_x and \dot{q}_y , respectively.

The orbital parameters are randomly chosen according to the observed properties of the young stellar ring. For all stars, the values for eccentricities are drawn from uniform random distribution between 0 and 0.3 (expecting that they will modestly self-excite during 6 My to values 0.3-0.4). Semi-major axes are randomly distributed between 6700 and 20100 au according to the $\propto r^{-1.4}$ surface density, and inclinations are chosen between 0 and 10° . Longitude of ascending node, argument of periapsis and true anomaly are drawn from uniform distributions between 0 and 2π . The set of initial conditions of one example simulation is shown in Fig.3.2.

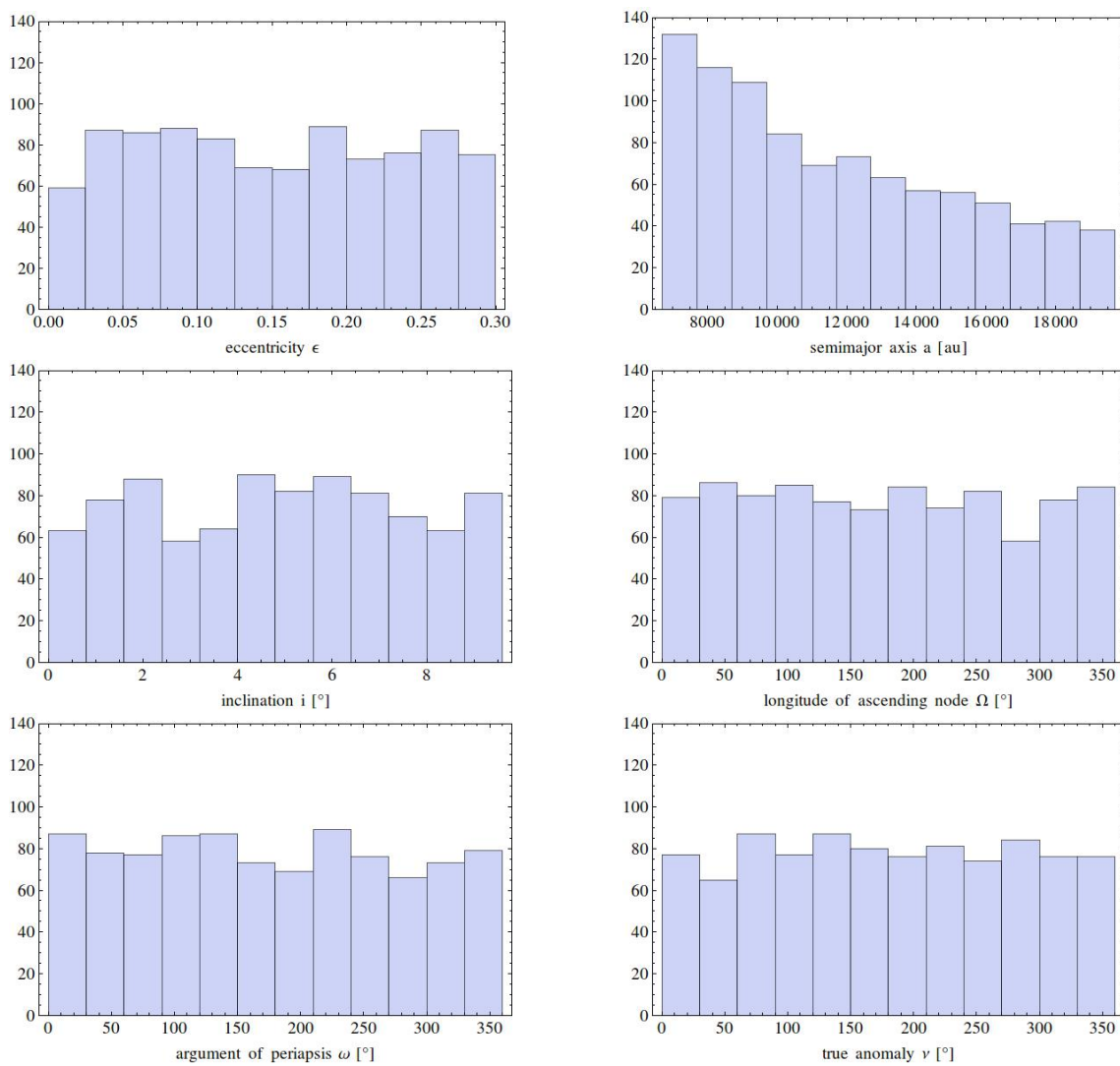


Fig. 3.2.: Histograms of initial conditions for one simulation (configuration I). From up to down: eccentricity, inclination, argument of periapsis (left column); semi-major axis, longitude of ascending node and true anomaly (right column).

3.5. Timestep

The Leapfrog integrator in REBOUND comes with a constant timestep. This ensures - if the timestep is small enough - energy conservation for the total system. The problem now is to find a timestep that on the one hand keeps the numerical errors sufficiently small. On the other hand computation time should stay in a realisable range. Press (1986) gives an estimation for an upper timestep limit to usefully extrapolate the motion of a particle in N-body simulations:

$$t_{\text{extrap}} = \frac{t_{\text{cross}}}{N^{\frac{1}{3}} \ln N} \quad (3.12)$$

with t_{cross} the crossing time which is needed by a typical star for a significant fraction of its orbit and N the number of stars in the system. In the case of the young stellar ring, $t_{\text{cross}} \sim 10^2$ yr and $N \sim 10^3$, resulting in $t_{\text{extrap}} \approx 1$ yr. But, this represents only an upper limit. It is still possible that if stars come very close their encounter is not resolved accurately. These encounters are indeed the most interesting events in the simulations as they can lead to strong scattering events bringing a star to a highly eccentric orbit. To ensure that also small encounter distances are accurately resolved I proceed as follows:

For the sake of computation time costs, first, test simulations including only the black hole and the perturber stars are conducted. Using a timestep of 1 yr, it can be observed that perturber stars self-excite in an unphysical way and a substantial fraction of stars is scattered out of the system (Fig.3.3, left panel). While reducing the timestep, the stars stay more and more stable until the eccentricities are only

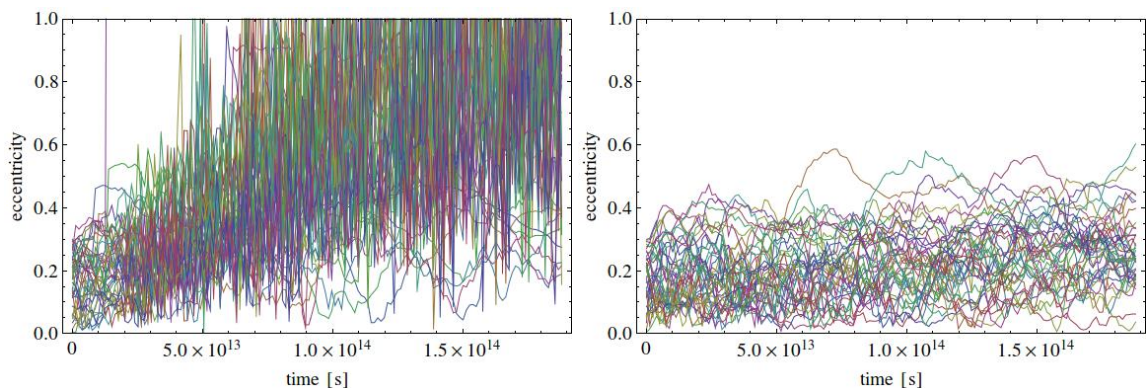


Fig. 3.3.: Evolution of eccentricities of perturber stars in simulations over 6 My with timestep $dt=1$ yr (left) and timestep $dt = 0.01$ yr (right) under identical initial conditions. Each colour corresponds to a different star.

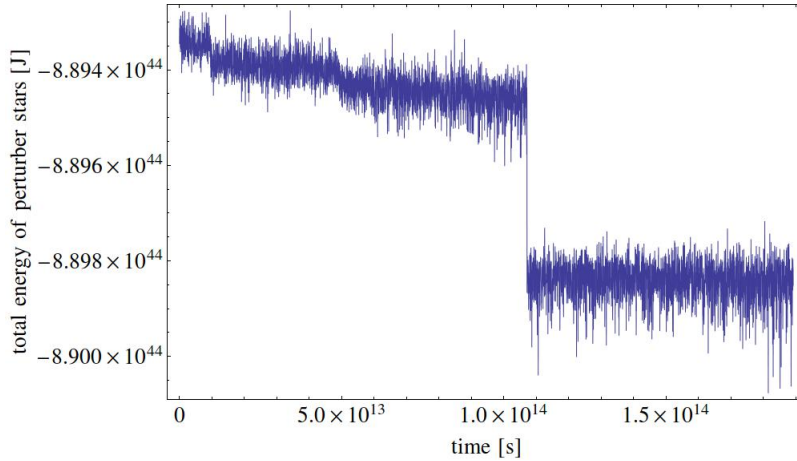


Fig. 3.4.: Evolution of total energy of perturber stars with timestep $dt = 0.01$ yr.

modestly excited with a timestep of $dt = 0.01$ yrs (Fig.3.3, right panel). Using this timestep, the total energy of perturber stars does show evidence of some unphysical discontinuity but the relative change is only of order 10^{-3} (see Fig.3.4.) So I choose this value as timestep for my simulations. It seems to be sufficiently accurate to evolve the perturber stars in a physical way, and the amount of computation time (~ 1 week when all 941 stars are included) is still in an acceptable range.

Nevertheless, it remains to check *which* close encounters distances are still resolved using this timestep and which are not. Therefore close encounter test simulations are conducted. I place a (non-moving) perturber star on the center and let a test particle move with a certain velocity and impact parameter in direction to the perturber. From the velocity output of the simulation I can calculate the scattering angle via $\cos(\theta) = \vec{v}_0 \cdot \vec{v}' / (|\vec{v}_0||\vec{v}'|)$ and compare it with the theoretical expected scattering angle from (2.2). As I also know how close the bodies will come during the scattering from $r_{min} = a(1 - \epsilon)$ with $a = \frac{\alpha}{2E}$, a correlation between the relative error in scattering angle dependent on velocity and closest approach distance for the chosen timestep can be derived. Varying relative velocities and impact parameters, I find that a minimal encounter distance of down to 2.5 au lead to relative errors of order 10^{-3} or smaller, which I consider as an acceptable limit for the moment (see Fig.3.5).

Now, the simulation are launched using $dt = 0.01$ yr including all particles, that means black hole, perturber stars and test particles. An additional function calculates and outputs the distances of every test particle to every perturber for each timestep. On this way it can be checked which particle gets closer to a perturber

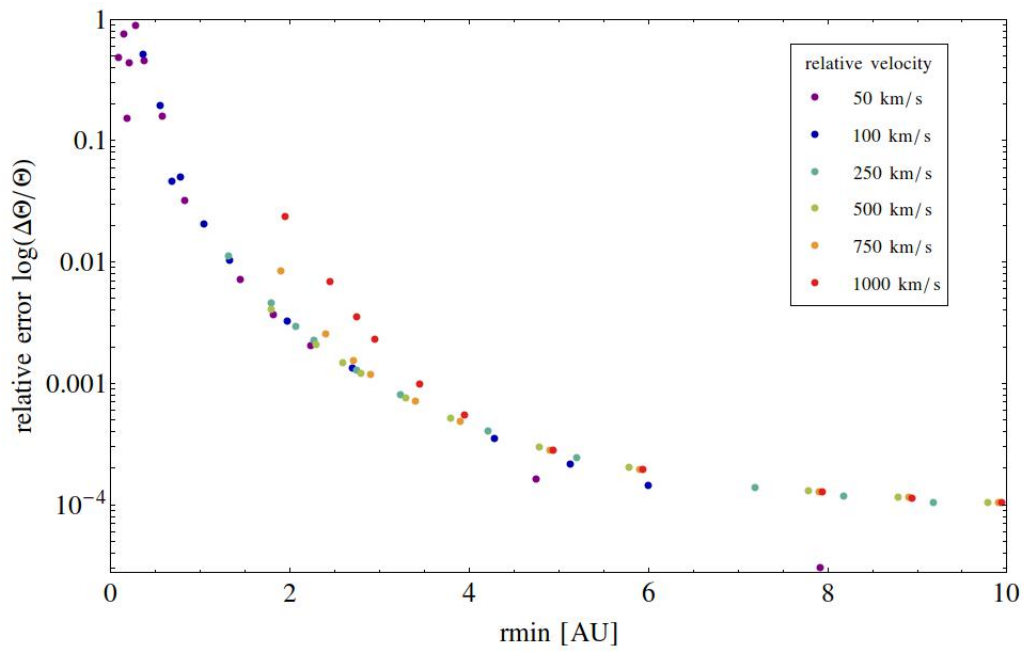


Fig. 3.5.: Plot of relative error in scattering angles at different encounter distances. Different colours refer to different velocities.

than the limit of 2.5 au and hence is expected to be calculated inaccurately.

3.6. Results

In total, I run 10 simulations with different random seeds for a total of 6 Myr. Results on dynamical properties can be seen in Fig.3.6 for one realisation, and in the appendix for the other simulations. The number of test particles scattered to G2-like orbits with $\epsilon > 0.9$ and $r_{\text{peri}} < 250$ au varies from simulation to simulation between 0 and 2. On average, 0.4 of 900 low-mass stars reach orbits fulfilling these criteria over the simulation lifetime. All of them can be observed on their highly eccentric orbits between 4 and 6 Myr. Further, a mean fraction of 0.4% of low-mass stars happen to be kicked out of the system, that means they reach $\epsilon > 1$.

The evaluation of the distances between perturbers and low-mass stars reveals that 10% of all test particles happens to have encounters with perturber stars at distances less than 2.5 au. Especially 95 % of the low mass stars that are kicked out of the ring ($\epsilon > 1$), and 3/4 of stars on G2-like orbits have experienced close encounters. Perturber stars stay – as expected – quite stable. Their mean eccentricity after 6 My reaches a value of 0.26, and inclinations result on average in 8.7° (see Table 3.1).

simulation	a	b	c	d	e	f	g
I (srand 81430)	2	1	2	2	82	0.27	8.0
II (srand 111820)	1	1	5	5	97	0.28	8.6
III (srand 1001)	0	0	3	3	93	0.22	7.8
IV (srand 91166)	0	0	2	2	81	0.22	8.8
V (srand 20280)	0	0	3	3	97	0.22	9.5
VI (srand 935991)	1	1	2	1	87	0.26	8.2
VII (srand 400087)	0	0	6	5	83	0.30	9.6
VIII (srand 5508428)	0	0	4	4	86	0.24	8.3
IX (srand 121290)	0	0	4	4	96	0.32	9.5
X (srand 599989)	0	0	5	5	75	0.24	8.5

Table 3.1.: Results of all 10 simulations. **(a)** number of test particles scattered on G2-like orbits, **(b)** number of particles in (a) that experience close encounters, **(c)** number of test particles kicked out of the system, **(d)** number of particles in (c) that experience close encounters, **(e)** number of all test particles experiencing close encounters < 2.5 au, **(f)** mean eccentricity of perturber stars after 6 My **(g)** mean inclination [$^\circ$] of perturber stars after 6 My.

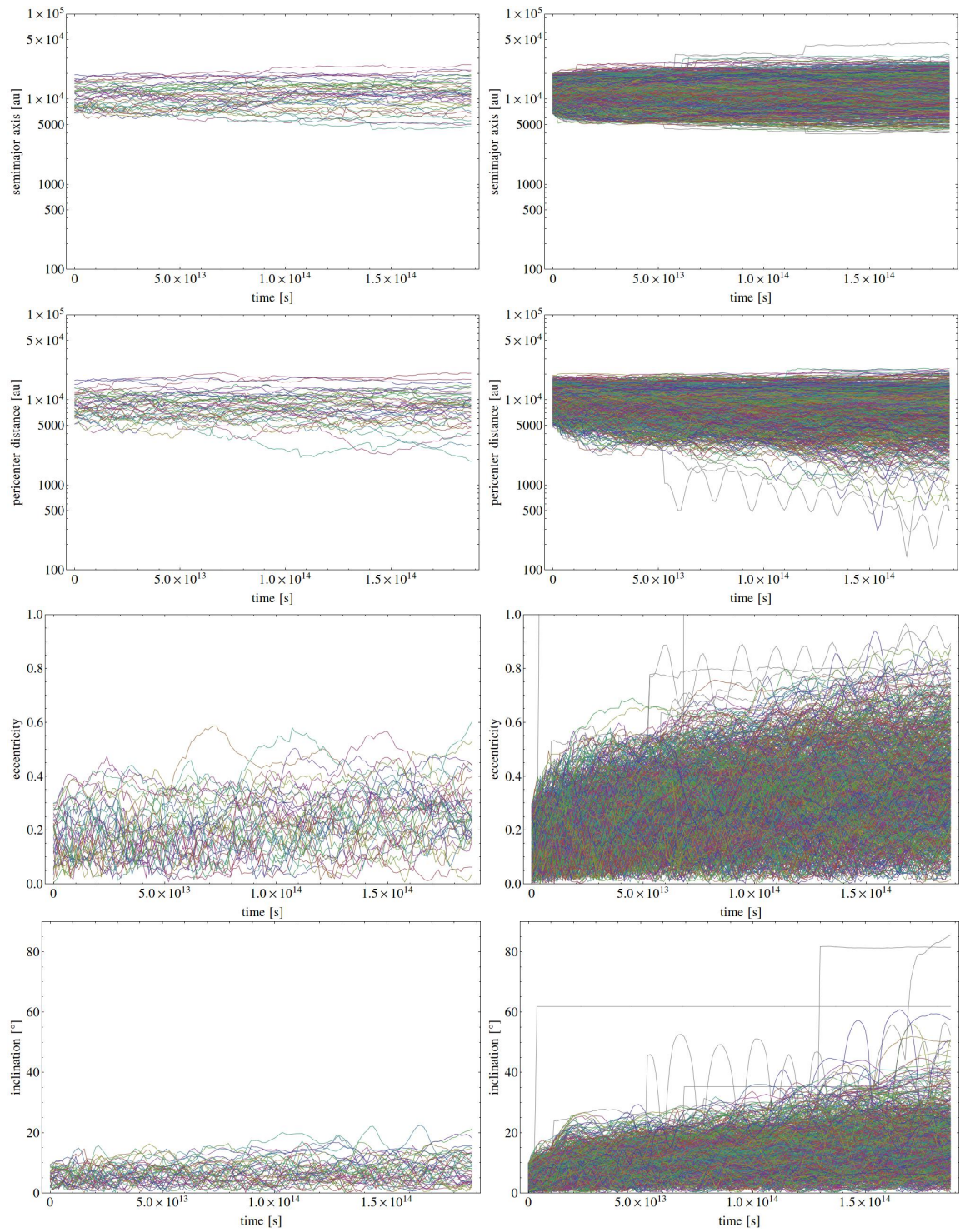


Fig. 3.6.: Evolution of semi-major axes, pericenter distances, eccentricities and inclinations for perturber stars (left column) and low-mass stars (right columns) of simulation configuration I. Each colour corresponds to one test particle. Low-mass stars that experience close encounters (< 2.5 au) are plotted in gray colour.

4. Discussion

4.1. Analytical calculations

The calculated scattering rate suggest that it is a very likely event to observe stars on G2-like orbits - if a hundred G2 clouds are traveling through the Galactic Center it should be nearly unlikely to *not* observe any of them. The point of delivery rates was already discussed by Murray-Clay and Loeb (2012); they computed rates of $6 \times 10^{-7} yr^{-1}$ for stars of mass $1M_{\odot}$ and one of $3 \times 10^{-6} yr^{-1}$ for such with mass $0.3M_{\odot}$ and which hence are a factor of about 6 smaller.

Still it is important to note that my approximations are very, if not too rough. First of all, the energy during three-body encounters is not conserved for each particle. For example, in space travel, nearby passages of space crafts on planets are used to speed up the vehicle relative to the sun (also called 'gravitational slingshot maneuver'). Giving up energy conservation has as consequence that the relation between ϵ'_* and scattering angle θ (equation 2.5) is not exact. By conducting several test simulations of three-body scattering it turned out that a scattering angle of at least 85° is necessary to scatter the low-mass star on a highly eccentric orbit. As a consequence, scattering and delivery rates may be diminished by a factor of 8. Then, numbers would come in a comparable range to that computed in Murray-Clay and Loeb (2012). Besides, scattering the star on a high eccentricity does not yet absolutely mean that it will have the same orbit as G2. Starting with radius (and hence semi-major axis) of 11000 au and assuming strict energy conservation for the low mass star, after scattering, it would end with an apocenter distance of $a(1 + \epsilon) \sim 22000$ au - twice the observed value. Consequently, either the star has to start with the half of its radius assuming energy conservation, that means with an initial radius of 5500 au, or energy loss has to be included in the theoretical considerations. The former appears to be very unlikely - observations suggest an very inner edge of the young stellar ring of ~ 6700 au. If G2 originates from farther inside, its link to the clockwise rotating disk can't be justified.

In total, the calculations give a first, upper limit for the delivery rate in the young stellar ring. Several considerations lead to the assumption that energy loss of the scattered star can't be neglected.

4.2. Simulation

4.2.1. Delivery rates and probabilities

On average, 0.4 of 900 test particles are scattered on G2-like orbits within 6 Myr corresponding to a delivery rate of $6.7 \times 10^{-8} \text{yr}^{-1}$. This lies about one order of magnitude below the delivery rates analytically calculated in Murray-Clay and Loeb (2012) (and significantly under that calculated in section 2.2.3, as expected). So you would have to wait for two times the age of the young stellar ring to get a probability of 80 % to observe at least one star on a G2-like orbit. Even if - with a probability of 40 % - one star is scattered to a highly eccentric orbit after 6 Myr, we have still to discover it, that means we have to watch on the right time the right part of the sky. So, all in all, my simulations let it be a quite unlikely event to observe G2 on its plunge towards the black hole. If G2 really hosts a star inside - we are somewhat fortunate to observe it. But, on the other hand it has to be noted that scattering to G2-like orbits seems to be *indeed* possible.

4.2.2. Single scattering encounters

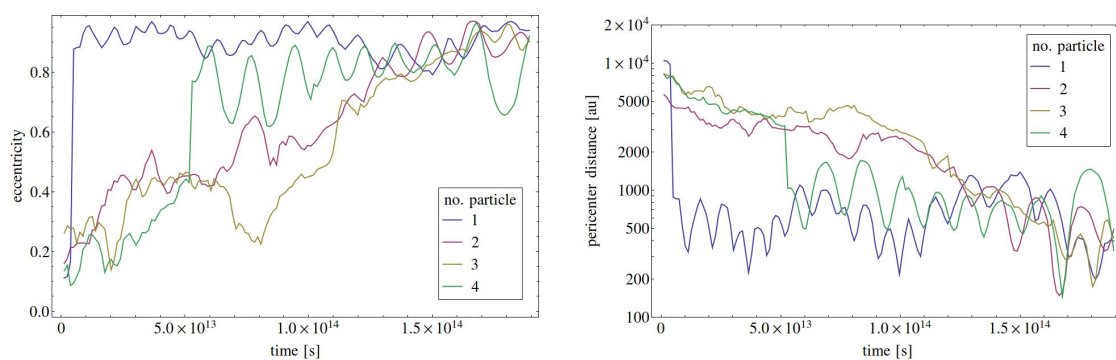


Fig. 4.1.: Evolution of eccentricities (left) and pericenter distances (right) of the four particles that are scattered on G2-like orbits in the total of the simulations.

Fig.4.1 shows the evolution of eccentricities and pericenter distances of the stars that reach highly eccentric orbits. It can be seen that one particle experiences a very strong encounter which transports it from an eccentricity of 0.2 to 0.9 and which diminishes pericenter distance by a factor of ten (blue line). Another particle experiences an encounter which transports it from an eccentricity of 0.4 to 0.8 (green line). Hence, strong scattering events seem to play some role in the dynamics of the young stellar ring, and even transporting a star to a low angular momentum orbit via one scattering encounter as discussed in section 2.2 seems to be indeed possible. The two other stars evolve quite constantly. It is only a question now if the strong scatterings can be considered as physical, or if there is some numerical error due to the choice of the timestep (see discussion 4.2.5, below) that produces the strong at-once scatterings.

4.2.3. Energy loss

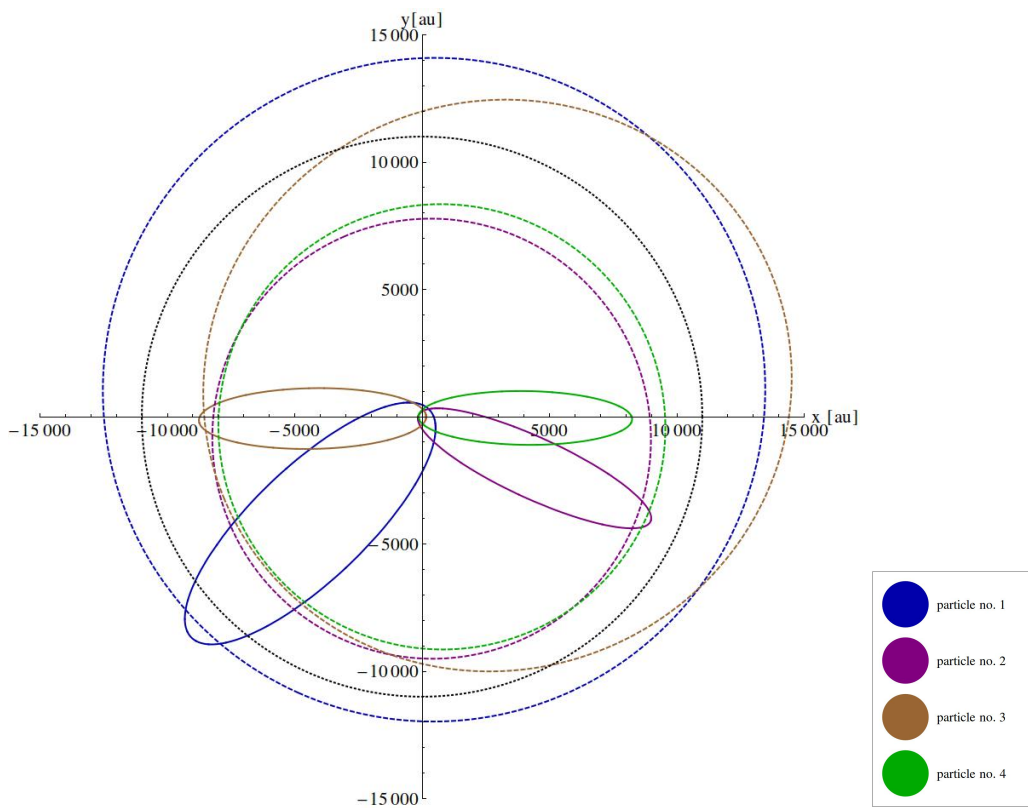


Fig. 4.2.: Final orbits of the 4 stars that in total reach G2-like orbits. Also their initial orbits are shown (dashed) and as well the cloud's proposed initial orbit at 11000 au (black, dotted).

In Fig. 4.2 can be seen the final and as well the initial orbits of the 4 highly eccentric low-mass stars produced in the simulations. As their final apocenter distances are in neighbourhood to their initial orbits, it follows that energy loss plays an important role during the scattering processes: $r_{\text{apo}} = a(1 + \epsilon) = \frac{\alpha}{2E}(1 + \epsilon)$, that means under the assumption of strict energy conservation, a significant change in ϵ would be followed by a significant change in r_{apo} . As their apocenter distances do not significantly change, energy cannot be conserved (see also discussion in 4.1). Indeed, all four low mass stars lose an amount of specific energy in the range of 170 - 230 %.

4.2.4. Dynamical properties of perturber stars

From Table 3.1 a mean eccentricity of 0.26 and a mean inclination of 8.7° for the perturber stars can be derived. These values lie slightly under the observed mean eccentricity of ~ 0.35 and the mean inclination of $\sim 10^\circ$ in the young stellar ring. This may have as reason either the choice of initial conditions (perhaps initial eccentricity between 0.1 and 0.3 would fit the observations on a better way than the values between 0 and 0.3 as used in the simulations). Besides, it could be possible that by further reducing the timestep scattering encounters are even better resolved and perturbers do more self-excite.

4.2.5. Accuracy of timestep

Despite all the accuracy tests which have been done before starting the simulations, there remains the problem that 10 % of all low-mass stars experience close encounters with distances less than 2.5 au. As shown in Fig.3.5, computation errors increase significantly at distances under the limit of 2.5 au. Even if the timestep of 0.01 yr seems to be appropriate for the perturber stars (relative energy change of total energy of perturber stars is of order 10^{-3} or less, in *each* simulation), numerous if not all of the test particles experiencing close encounters could be computed incorrectly. Hence, the next step to improve accuracy should be to find a smaller timestep which brings the dynamics of these particles to convergence. This could be done by running simulations including only black hole, perturber stars and the close encounter test particles using timesteps that are reduced step by step. One could compare final orbital parameters or positions of each timestep and decide for the timestep at which the relative difference in some parameter is for example of order 10^{-3} relative to the

next bigger timestep. When $\sim 10\%$ of all particles are included, simulations should run substantially faster and also with smaller timesteps computation time could stay in an acceptable range.

By conducting the three-body simulations mentioned in section 4.1, I could see that at very small impact parameters the test particle can be kicked out of the system using a larger timestep, but remains bound to the system using some smaller timestep. As 95% of the kicked out stars in my simulations have experienced close encounters I expect that less or even no particle is kicked out at convergent timestep. Due to their small encounter distance they could then experience strong scatterings that might bring them on highly eccentric orbits instead being kicked out. This could increase the delivery rate determined above.

It should be noted that Murray-Clay and Loeb (2012) compute a minimum encounter distance of about ~ 10 au to ensure that the protoplanetary disks in their model stays safe from disruption. As 3/4 highly eccentric stars suffer close encounters at 2.5 au or less it is clear that the probability of observing G2 as a photoevaporating disk further shrinks from my simulations.

Summary

The Galactic Centre gas cloud G2 is moving towards the black hole of our Milky Way on a highly eccentric, low angular momentum orbit. Two models presented by Murray-Clay and Loeb (2012) and Scoville and Burkert (2013) assume a low-mass star as source for the observed cloud which could have been scattered by perturber stars of the young stellar ring to its unusual orbit. In this bachelor thesis I focused on the question of the likelihood for a low-mass star originating from the disk of young stars in the Galactic Centre to be scattered on a G2-like orbit.

First, I made a rough analytical approximation on the delivery rates on highly eccentric orbits by one single scattering event assuming that energy for each particle is conserved and that the scattering takes place for an infinitely short time. As a result, about 20-100 low-mass stars could reach G2-like orbits on that way, depending on their mass. This would represent a quite likely event. Though, the approximations used for the calculations turned out not to match the simulated conditions of scattering processes in a three-body problem; especially the assumption of energy conservation for each particle seems not to be justified. Hence, these approximations are not appropriate to get reliable and accurate results.

As a consequence I run 10 N-body simulations with different initial conditions imitating the evolution of the young stellar ring. On average, 0.4 of 900 low-mass stars are scattered on a G2-like orbit within 6 My which is in strong contrast to the analytical result. This means a very low probability to get scattered into the Galactic Centre. Further, it could be shown from the simulations that energy loss indeed plays an important role during scattering processes, and that stars indeed can be scattered onto the highly eccentric orbits by one scattering event as considered in the analytical approach.

But also simulations are imperfect: it is to notice that the chosen timestep does not seem to provide convergence for the test particles yet. 10 % of the low mass stars get close encounters that cannot be resolved on a reliable way. It is a future task to find an appropriate timestep and to resimulate the particles that suffer too close

scatterings. I expect the probability to get scattered on highly eccentric orbits to increase while approaching convergence.

But all in all, independent of any delivery rate or scattering probability - we *do* observe a gas cloud on a highly unusual orbit. And if there is really a star embedded inside - at the latest in a few years from now after pericenter passage we will know more about it. Even though the physics of a black hole and its accretion flow in reality doesn't have anything to do with that of its popular status as a 'cosmic vacuum cleaner', there will take place a significant interaction with G2 which could reveal its nature. In any case, if the cloud is still observable after pericenter passage, this would be a clear hint that the stellar source models could be very close to reality.

Acknowledgements

First of all, I would like to thank Prof. Dr. Andreas Burkert for the opportunity to work on this exciting and fascinating project. The frequent meetings with stimulating and helpful discussions contributed significantly to a successful progress in my work. I am very grateful to him for having me completely and openly included in the CAST group. I enjoyed it a lot to work in this pleasant environment and benefited from the excellent specialist knowledge and the great commitment of all the group members.

I would also like to express my special thank to Dr. Marc Schartmann. He was always ready to help me with physical and technical questions. Further, his high level commitment in proofreading this bachelor thesis was of great importance for me to revise this work - not only with regard to specialist but also to linguistic and formal terms.

Furthermore, Christian Alig provided very helpful programming assistance and took a lot of time for helping me with occurring problems - thanks a lot for your support!

Working on this bachelor project gave me a great time and allowed me to learn about handling scientific problems, to apply computational tools as well as to write a scientific publication. Thank you to all parties concerned!

A. Appendix

In the plots of Fig.A.1 to Fig.A.9 can be seen dynamical properties (evolution of semimajor axes, pericenter distances, eccentricities and inclinations) of perturber stars (left columns) and low-mass stars (right columns) for the initial configurations II-X. Each line and colour corresponds to one star. Gray lines are associated with low-mass stars that have experienced close encounters with perturbers at distances < 2.5 au.

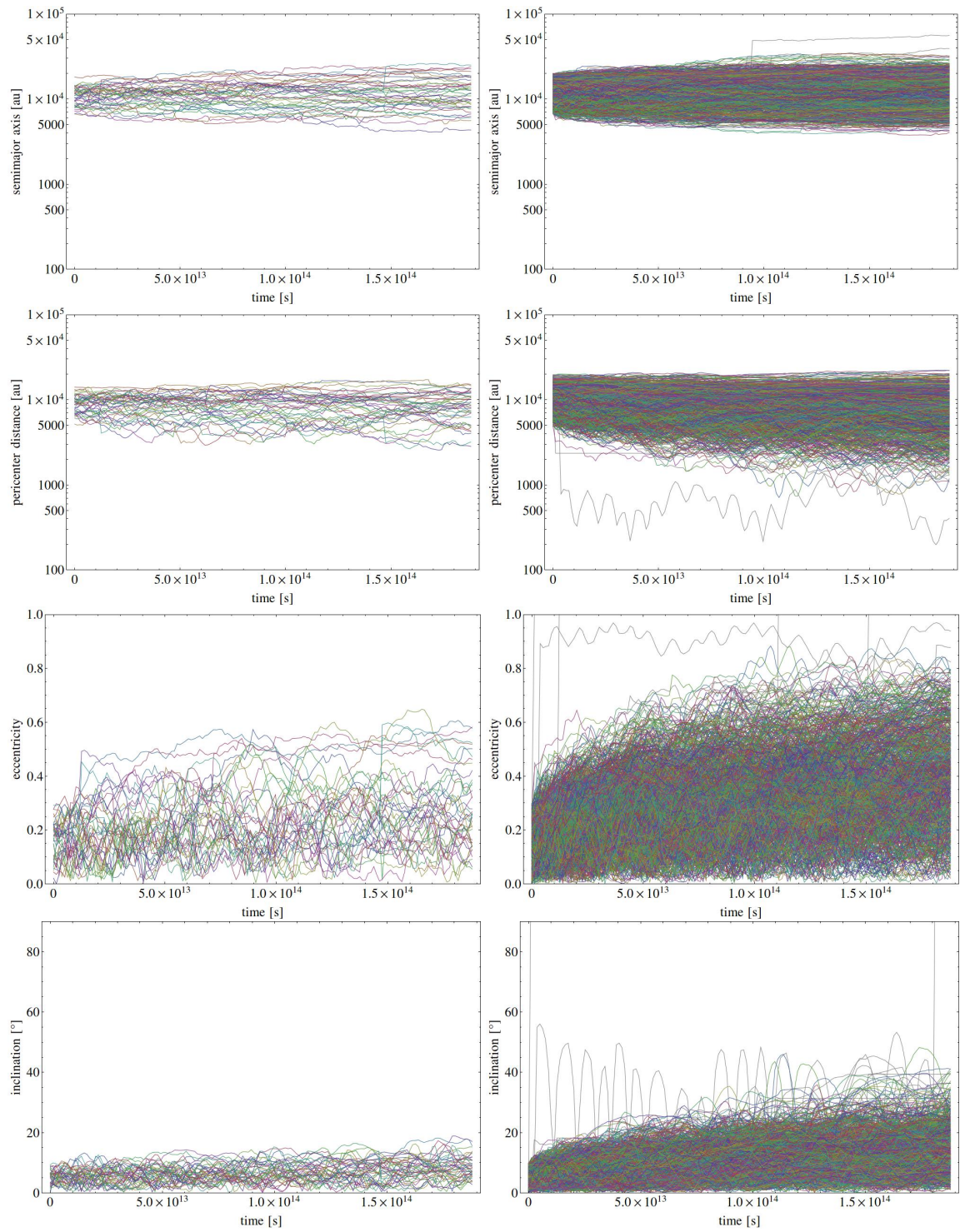


Fig. A.1.: Evolution of semi-major axes, pericenter distances, eccentricities and inclinations for perturber stars (left column) and low-mass stars (right columns) of simulation configuration II. Each colour corresponds to one test particle. Low-mass stars that experience close encounters (< 2.5 au) are plotted in gray colour.

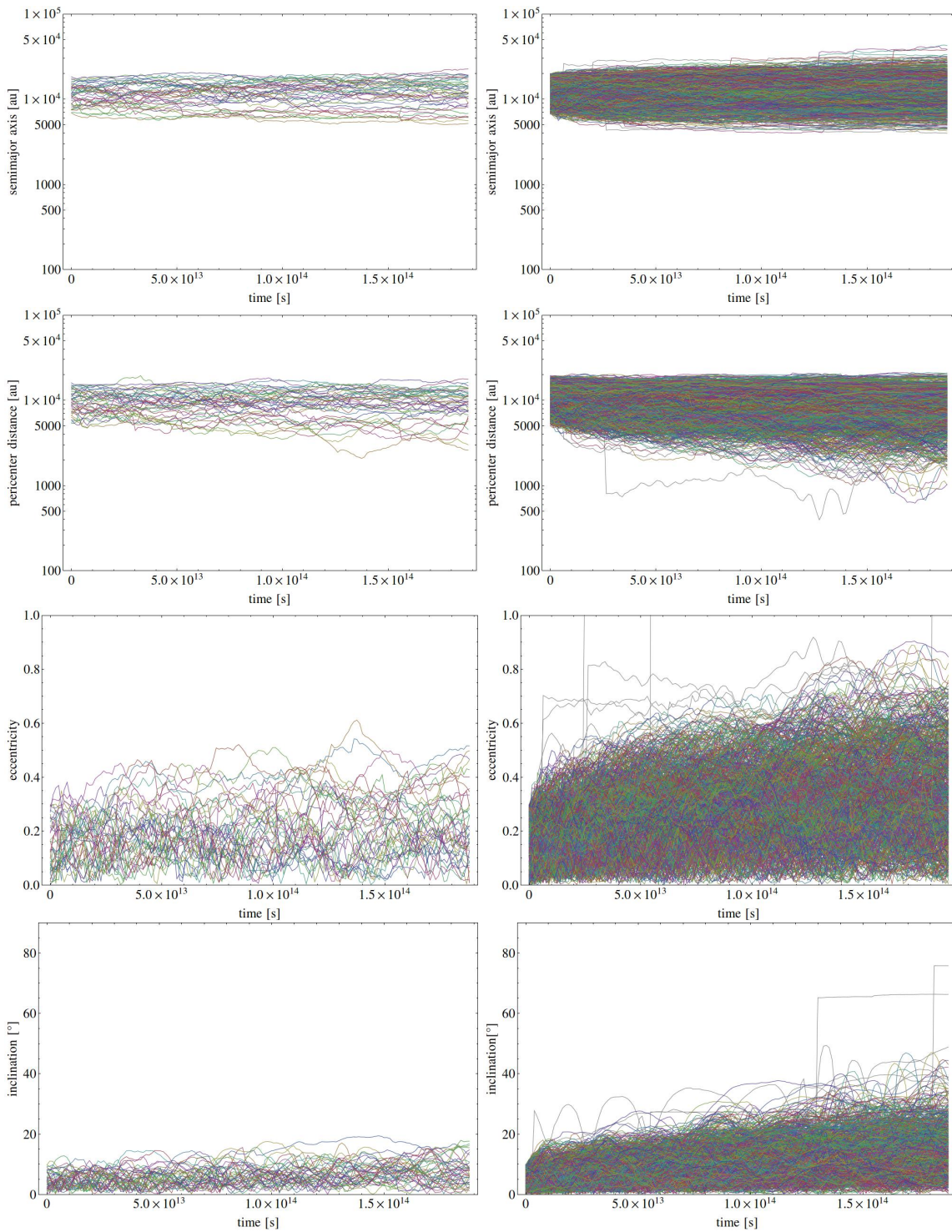


Fig. A.2.: Evolution of semi-major axes, pericenter distances, eccentricities and inclinations for perturber stars (left column) and low-mass stars (right columns) of simulation configuration III. Each colour corresponds to one test particle. Low-mass stars that experience close encounters (< 2.5 au) are plotted in gray colour.

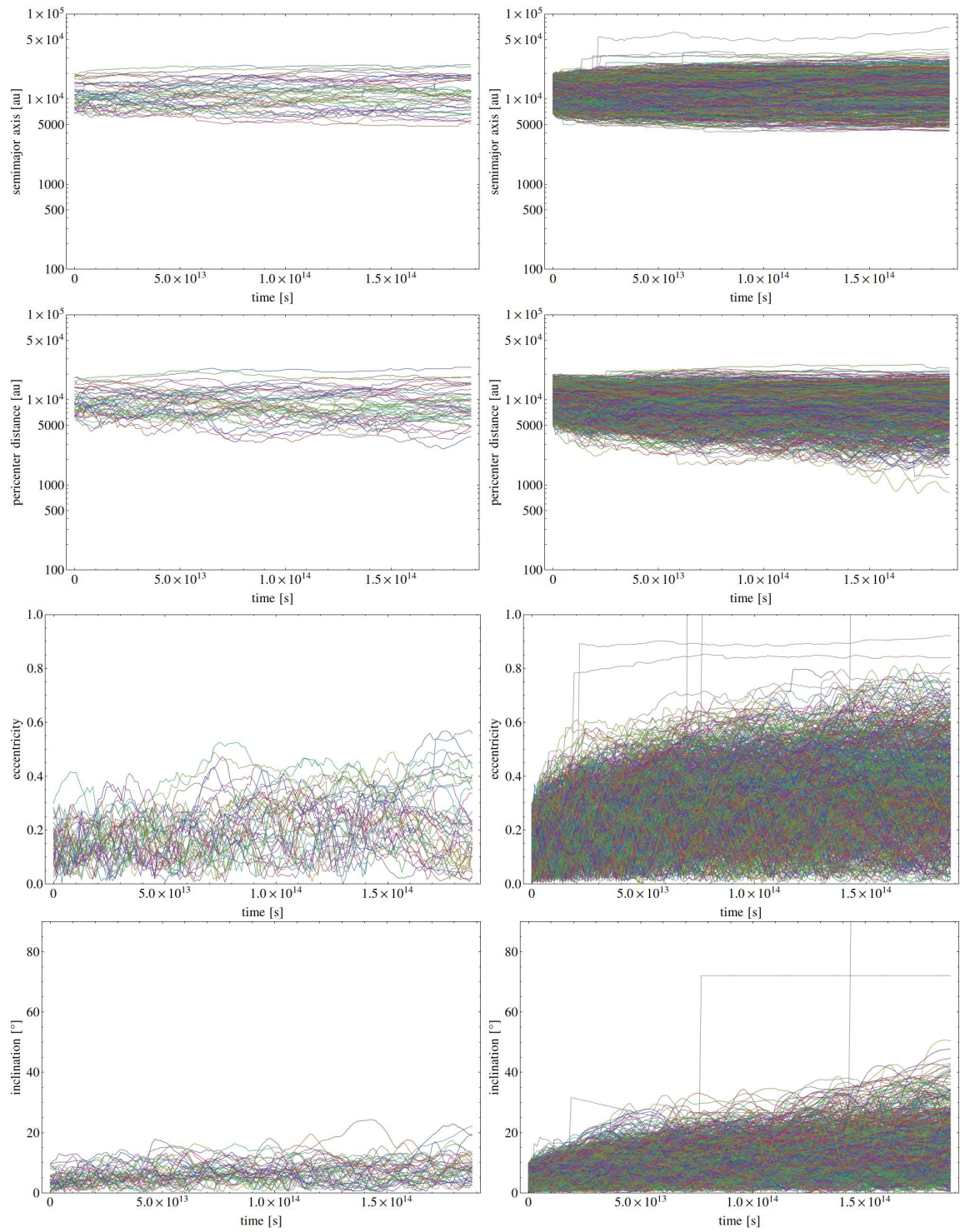


Fig. A.3.: Evolution of semi-major axes, pericenter distances, eccentricities and inclinations for perturber stars (left column) and low-mass stars (right columns) of simulation configuration IV. Each colour corresponds to one test particle. Low-mass stars that experience close encounters (< 2.5 au) are plotted in gray colour.

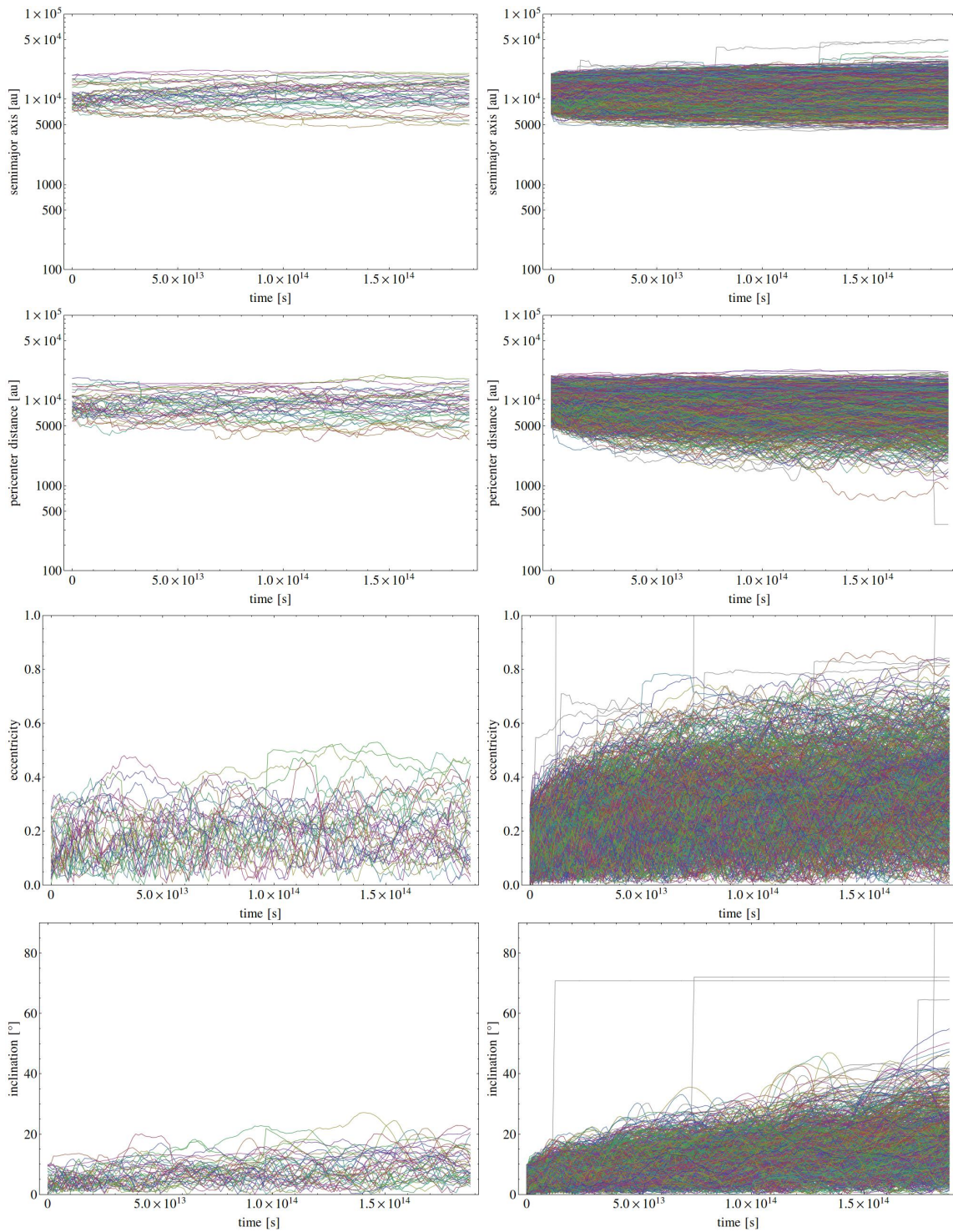


Fig. A.4.: Evolution of semi-major axes, pericenter distances, eccentricities and inclinations for perturber stars (left column) and low-mass stars (right columns) of simulation configuration V. Each colour corresponds to one test particle. Low-mass stars that experience close encounters (< 2.5 au) are plotted in gray colour.

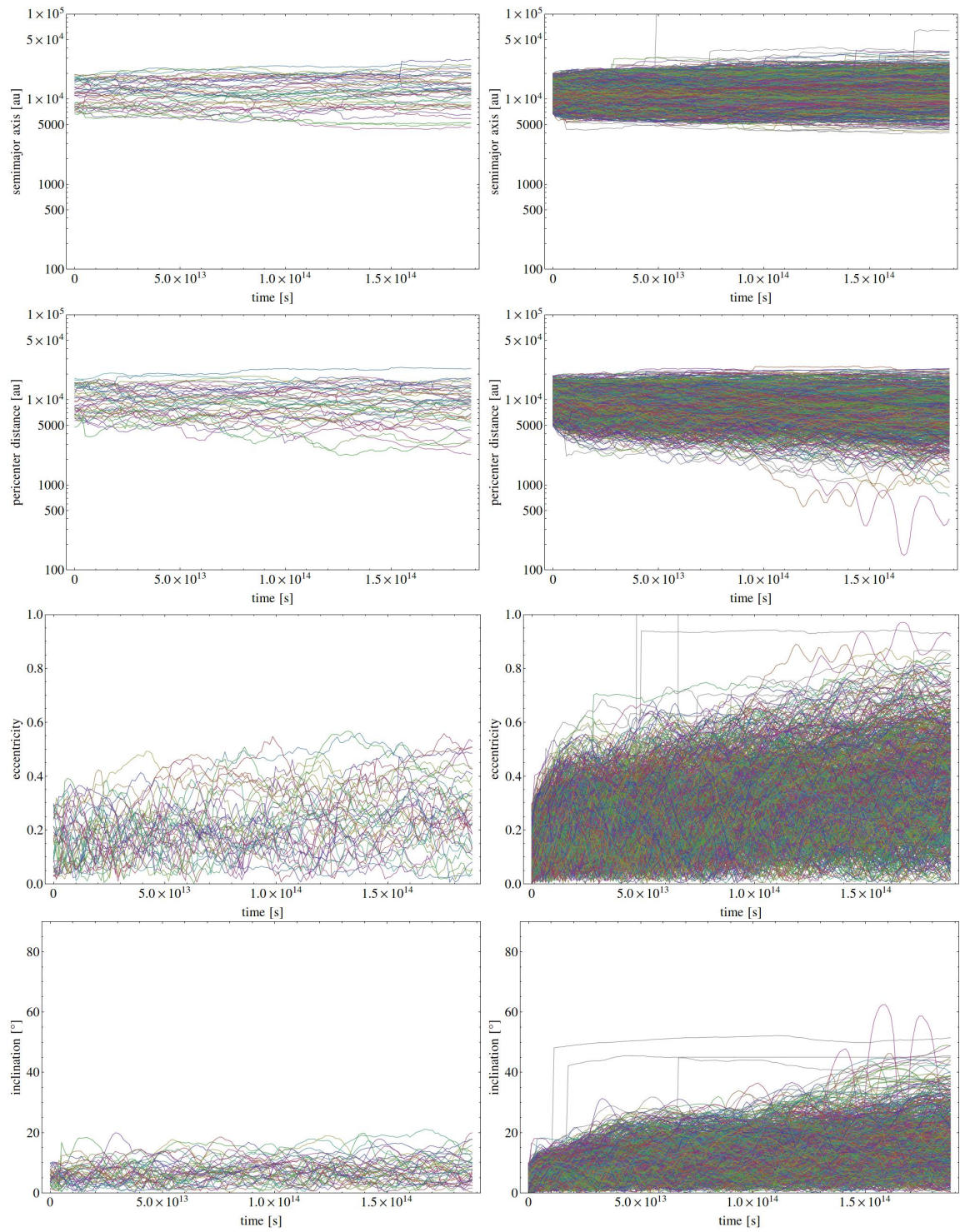


Fig. A.5.: Evolution of semi-major axes, pericenter distances, eccentricities and inclinations for perturber stars (left column) and low-mass stars (right columns) of simulation configuration VI. Each colour corresponds to one test particle. Low-mass stars that experience close encounters (< 2.5 au) are plotted in gray colour.

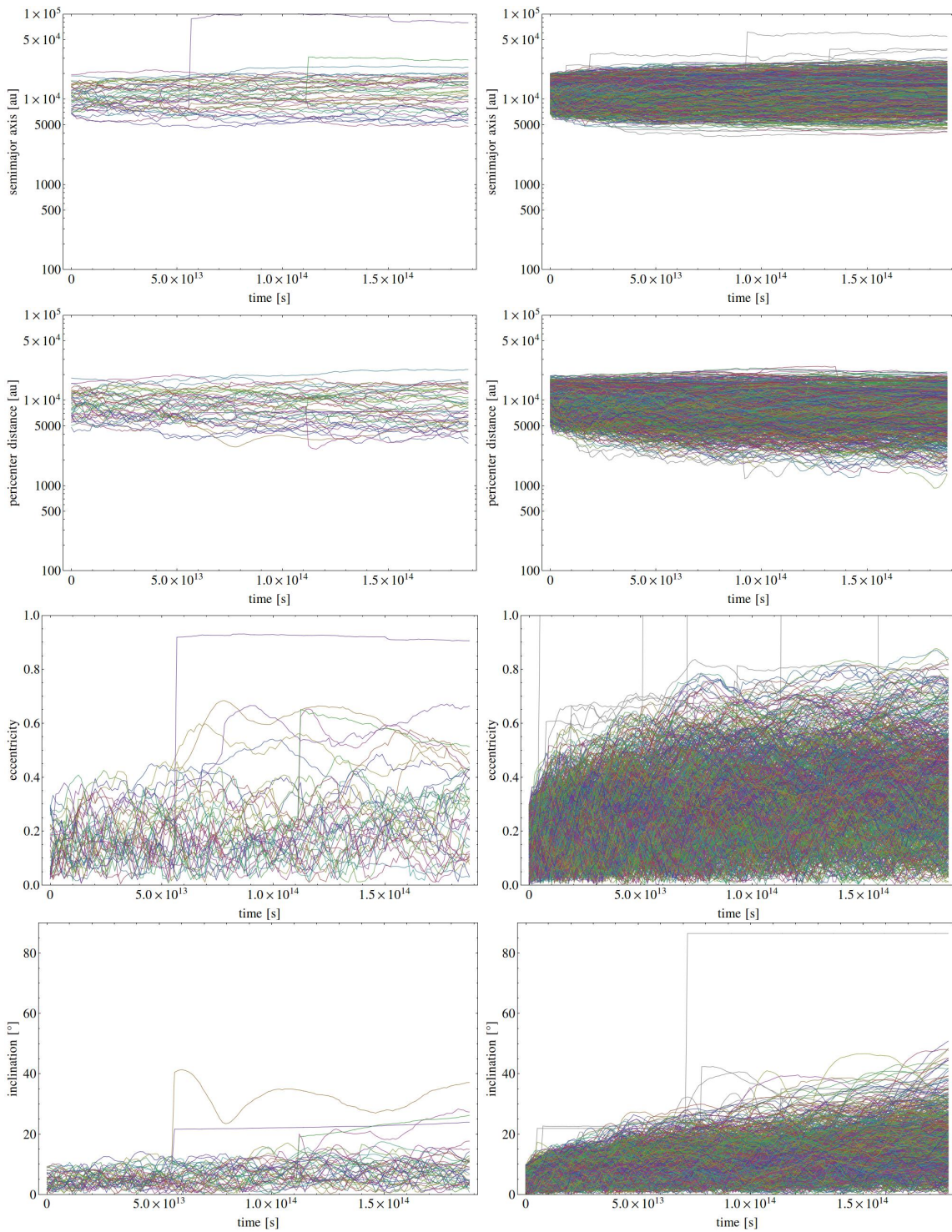


Fig. A.6.: Evolution of semi-major axes, pericenter distances, eccentricities and inclinations for perturber stars (left column) and low-mass stars (right columns) of simulation configuration VII. Each colour corresponds to one test particle. Low-mass stars that experience close encounters (< 2.5 au) are plotted in gray colour.

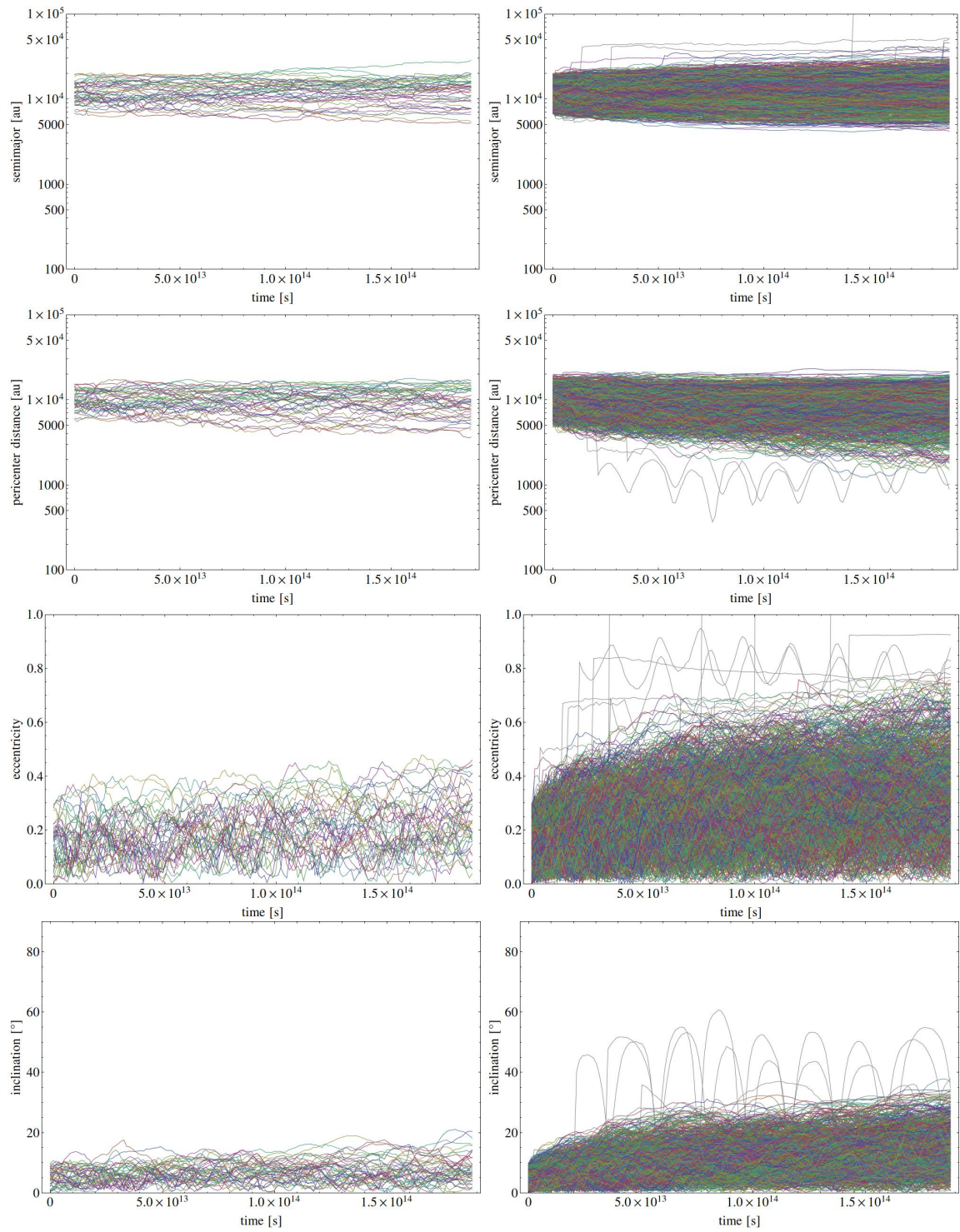


Fig. A.7.: Evolution of semi-major axes, pericenter distances, eccentricities and inclinations for perturber stars (left column) and low-mass stars (right columns) of simulation configuration VIII. Each colour corresponds to one test particle. Low-mass stars that experience close encounters (< 2.5 au) are plotted in gray colour.

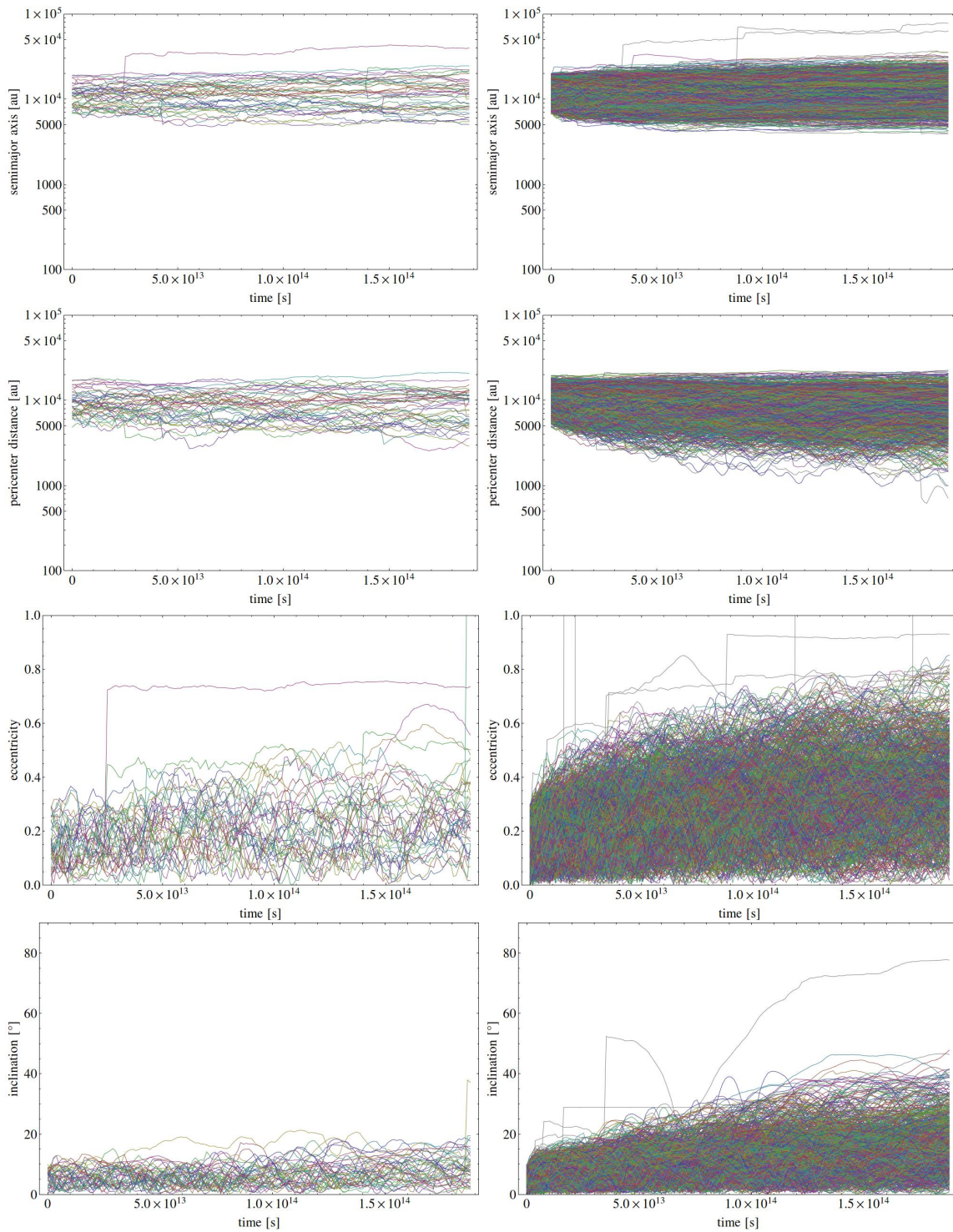


Fig. A.8.: Evolution of semi-major axes, pericenter distances, eccentricities and inclinations for perturber stars (left column) and low-mass stars (right columns) of simulation configuration IX. Each colour corresponds to one test particle. Low-mass stars that experience close encounters (< 2.5 au) are plotted in gray colour.

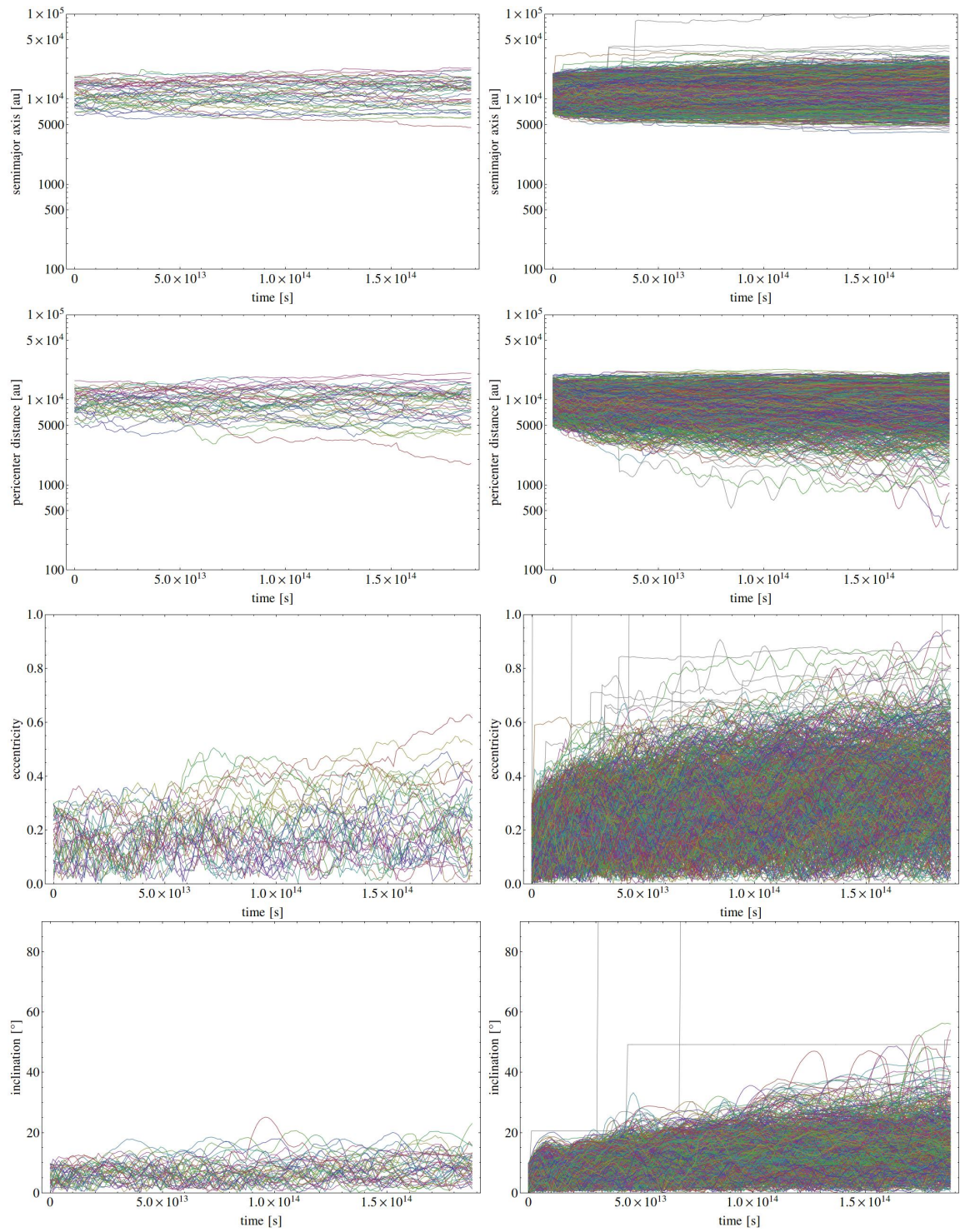


Fig. A.9.: Evolution of semi-major axes, pericenter distances, eccentricities and inclinations for perturber stars (left column) and low-mass stars (right columns) of simulation configuration X. Each colour corresponds to one test particle. Low-mass stars that experience close encounters (< 2.5 au) are plotted in gray colour.

Bibliography

- Alexander, T. (2005). Stellar processes near the massive black hole in the Galactic center [review article]. *Physics Reports*, 419:65–142.
- Alig, C., Burkert, A., Johansson, P. H., and Schartmann, M. (2011). Simulations of direct collisions of gas clouds with the central black hole. *Monthly Notices of the Royal Astronomical Society*, 412:469–486.
- Alig, C., Schartmann, M., Burkert, A., and Dolag, K. (2013). Numerical Simulations of the Possible Origin of the Two Sub-parsec Scale and Counterrotating Stellar Disks around SgrA*. *The Astrophysical Journal*, 771:119.
- Bartko, H., Martins, F., Fritz, T. K., Genzel, R., Levin, Y., Perets, H. B., Paumard, T., Nayakshin, S., Gerhard, O., Alexander, T., Dodds-Eden, K., Eisenhauer, F., Gillessen, S., Mascetti, L., Ott, T., Perrin, G., Pfuhl, O., Reid, M. J., Rouan, D., Sternberg, A., and Trippe, S. (2009). Evidence for Warped Disks of Young Stars in the Galactic Center. *The Astrophysical Journal*, 697:1741–1763.
- Binney, J. and Tremaine, S. (2008). *Galactic Dynamics: Second Edition*. Princeton University Press.
- Bonnell, I. A. and Rice, W. K. M. (2008). Star Formation Around Supermassive Black Holes. *Science*, 321:1060–.
- Burkert, A., Schartmann, M., Alig, C., Gillessen, S., Genzel, R., Fritz, T. K., and Eisenhauer, F. (2012). Physics of the Galactic Center Cloud G2, on Its Way toward the Supermassive Black Hole. *The Astrophysical Journal*, 750:58.
- Dehnen, W. and Read, J. I. (2011). N-body simulations of gravitational dynamics. *European Physical Journal Plus*, 126:55.
- Fliessbach, T. (2009). *Mechanik*. Spektrum Akademischer Verlag.

- Genzel, R., Eisenhauer, F., and Gillessen, S. (2010). The Galactic Center massive black hole and nuclear star cluster. *Reviews of Modern Physics*, 82:3121–3195.
- Gillessen, S., Eisenhauer, F., Trippe, S., Alexander, T., Genzel, R., Martins, F., and Ott, T. (2009). Monitoring Stellar Orbits Around the Massive Black Hole in the Galactic Center. *The Astrophysical Journal*, 692:1075–1109.
- Gillessen, S., Genzel, R., Fritz, T. K., Eisenhauer, F., Pfuhl, O., Ott, T., Cuadra, J., Schartmann, M., and Burkert, A. (2013a). New Observations of the Gas Cloud G2 in the Galactic Center. *The Astrophysical Journal*, 763:78.
- Gillessen, S., Genzel, R., Fritz, T. K., Eisenhauer, F., Pfuhl, O., Ott, T., Schartmann, M., Ballone, A., and Burkert, A. (2013b). Pericenter passage of the gas cloud G2 in the Galactic Center. *ArXiv e-prints*.
- Gillessen, S., Genzel, R., Fritz, T. K., Quataert, E., Alig, C., Burkert, A., Cuadra, J., Eisenhauer, F., Pfuhl, O., Dodds-Eden, K., Gammie, C. F., and Ott, T. (2012). A gas cloud on its way towards the supermassive black hole at the Galactic Centre. *Nature*, 481:51–54.
- Haisch, Jr., K. E., Lada, E. A., and Lada, C. J. (2001). Disk Frequencies and Lifetimes in Young Clusters. *The Astrophysical Journal*, 553:L153–L156.
- Hut, P., Makino, J., and McMillan, S. (1995). Building a better leapfrog. *The Astrophysical Journal*, 443:L93–L96.
- Landau, L. D. and Lifshitz, E. M. (1966). *Mechanik*.
- Latter, H. N., Rein, H., and Ogilvie, G. I. (2012). The gravitational instability of a stream of co-orbital particles. *Monthly Notices of the Royal Astronomical Society*, 423:1267–1276.
- Meyer, F. and Meyer-Hofmeister, E. (2012). A nova origin of the gas cloud at the Galactic center? *Astronomy & Astrophysics*, 546:L2.
- Murray-Clay, R. A. and Loeb, A. (2012). Disruption of a proto-planetary disc by the black hole at the milky way centre. *Nature Communications*, 3.

- Natta, A. (2004). Circumstellar Disks in Pre-Main Sequence Stars. In Caroff, L., Moon, L. J., Backman, D., and Praton, E., editors, *Debris Disks and the Formation of Planets*, volume 324 of *Astronomical Society of the Pacific Conference Series*, page 20.
- Paardekooper, S.-J., Rein, H., and Kley, W. (2013). The formation of systems with closely spaced low-mass planets and the application to Kepler-36. *ArXiv e-prints*.
- Phifer, K., Do, T., Meyer, L., Ghez, A. M., Witzel, G., Yelda, S., Boehle, A., Lu, J. R., Morris, M. R., Becklin, E. E., and Matthews, K. (2013). Keck Observations of the Galactic Center Source G2: Gas Cloud or Star? *The Astrophysical Journal*, 773:L13.
- Press, W. H. (1986). Techniques and Tricks for N-Body Computation. In Hut, P. and McMillan, S. L. W., editors, *The Use of Supercomputers in Stellar Dynamics*, volume 267 of *Lecture Notes in Physics*, Berlin Springer Verlag, page 184.
- Rein, H. and Latter, H. N. (2013). Large-scale N-body simulations of the viscous overstability in Saturn's rings. *Monthly Notices of the Royal Astronomical Society*, 431:145–158.
- Rein, H. and Liu, S.-F. (2012). REBOUND: an open-source multi-purpose N-body code for collisional dynamics. *Astronomy & Astrophysics*, 537:A128.
- Schartmann, M., Burkert, A., Alig, C., Gillessen, S., Genzel, R., Eisenhauer, F., and Fritz, T. K. (2012). Simulations of the Origin and Fate of the Galactic Center Cloud G2. *The Astrophysical Journal*, 755:155.
- Scoville, N. and Burkert, A. (2013). The Galactic Center Cloud G2: A Young Low-mass Star with a Stellar Wind. *The Astrophysical Journal*, 768:108.
- Wikipedia (2010). Wikipedia, aufgerufen am: 10.07.2013. <https://en.wikipedia.org/wiki/File:Orbit1.svg>.

List of Figures

0.1. Observations of G2 in different wavebands	2
0.2. Position-velocity diagrams of G2	3
1.1. Schematic illustrations on model by Murray-Clay & Loeb	8
1.2. Schematic illustration on model by Scoville & Burkert	10
2.1. Sketch of bound, Keplerian orbit	12
2.2. Sketch of hyperbolic orbit	12
2.3. Schematic illustration on 3-body scattering approximation	14
2.4. Plot of mass fractions in the young stellar ring	16
3.1. Visualization of orbital elements of Keplerian orbit	21
3.2. Histograms of initial conditions	23
3.3. Evolution of eccentricities using different timesteps	24
3.4. Evolution of total energy of perturber stars	25
3.5. Plot of relative error in scattering angle at close encounter tests	26
3.6. Dynamical properties of stars in simulation I	28
4.1. Eccentricities and pericenter distances of stars on G2-like orbits	30
4.2. Orbits of stars on G2-like orbits	31
A.1. Dynamical properties of stars in simulation II	40
A.2. Dynamical properties of stars in simulation III	41
A.3. Dynamical properties of stars in simulation IV	42
A.4. Dynamical properties of stars in simulation V	43
A.5. Dynamical properties of stars in simulation VI	44
A.6. Dynamical properties of stars in simulation VII	45
A.7. Dynamical properties of stars in simulation VIII	46
A.8. Dynamical properties of stars in simulation IX	47
A.9. Dynamical properties of stars in simulation X	48

Statement of self-reliance

I hereby confirm

that I have written the present thesis independently and without illicit assistance from third parties and using solely the aids mentioned. I am aware that infringement may lead to the deprivation of the academic qualification subsequently.

Munich, August 12th, 2013

place, date

signature